Design and Optimisation of a Propeller for a Micro Air Vehicle Using Computational Fluid Dynamics

Ryan S.A. Turner[1]

University of New South Wales at the Australian Defence Force Academy

The purpose of this investigation is to design and optimise a propeller for use on a micro-air vehicle (MAV). The MAV in question weighs 150g, with a wingspan of 0.15m and operates at a forward flight speed of 11.0ms^{-1}. The thrust requirement of the propeller for these parameters was estimated at 0.24N using various drag estimation methods. The low chord-Reynolds number (*Re*) regimes encountered in MAV flight, create major challenges in designing efficient propellers and wings, due to the increased dominance of viscous forces and laminar boundary-layer separation. The aerodynamic parameters studied include the effect of changing Re, airfoil thickness, camber percentage and position, angle of attack for maximum *L/D*, propeller diameter, geometric pitch distribution and number of blades. 2D airfoil and 3D propeller models were analysed and optimised in the computational fluid dynamics (CFD) program FLUENT in order to yield the maximum airfoil lift to drag ratio (*L/D)* and propeller efficiency respectively. The highest propeller efficiency achieved by a design which satisfied the thrust requirement was 60.7%. The final design was an 8-cm diameter propeller using a NACA2309 airfoil operating at 20,000RPM. It was found that airfoil and propeller performance deteriorated significantly for $Re < 30{,}000$ and that use of cambered airfoils yielded significant improvements in *L/D* and propeller thrust on torque (*T/Q*). Propeller efficiency increased as diameter (*D*) was reduced, due to reductions in blade loading, and efficiency decreased significantly with increasing number of blades (*B*), due to the low advance ratio regimes in which the propellers were tested.

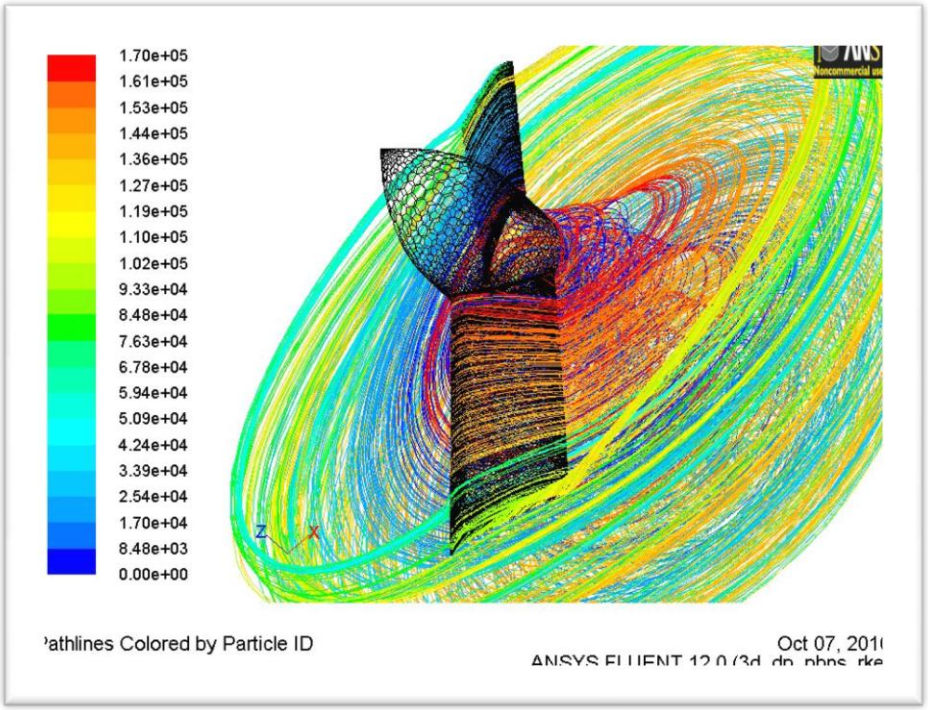

[1] OFFCDT, School of Engineering & Information Technology. ZEIT 4500 Aeronautical Thesis & Practical Experience.

Table of Contents

APPENDICES

Nomenclature

AR = aspect ratio, b^2/S
B = number of propeller blades
c = propeller blade / wing chord length [m]
J = advance ratio parameter
N = revolutions per minute [RPM]
n = revolutions per second [rps]
p = atmospheric pressure [in-Hg]
P_{bl} = propeller blade loading [W/ m^2]
P_p = power produced by propeller [W]
P_M = power produced by motor [W]
q = dynamic pressure [lb/ft^2]
Q = torque [in-lb]
Re = Reynolds number
r = propeller radius [m]
T = thrust [lb]
V_a = advance velocity [m/s]
W_{to} = MAV take-off weight [g or kg]
Ω = rotational velocity [rad/s]
ρ = density [slugs/ft^3]
ω = rotational velocity [rad/s]
η_p = propeller efficiency
μ = dynamic viscosity [Pa.s]

I. Introduction

The battlefield demand for surveillance and targeting has led to the development of small unmanned aerial vehicles known as Micro-air vehicles (MAVs). This project requires the investigation low-Re aerodynamics and the testing of small-scale propellers in order to produce a design suitable for use on a MAV. The genesis of the development of these platforms dates from 1996, with a proposal for aircraft carrying visual, acoustic, chemical or biological sensors (1). Interest in MAV development has increased over the years, with the award of many defence contracts and related industry and university studies. Demand for these platforms is likely to continue to increase as the platforms prove their utility across many missions and in many theatres. It has been reported that the most requested asset in the operational theatres of Afghanistan and Iraq is in fact the UAV (2). The Association for Unmanned Vehicles Systems International (AUVSI) defines micro UAVs as those with maximum weights up to 2 lbs (907.2 g), however the focus of this study is on a MAVs with a take-off weight of 150g and a wingspan of 0.15m. Their low cost and low probability of being detected means that MAVs provide a cost-effective surveillance alternative for many mission profiles when compared to larger vehicles.

Due to their size, the major limitation of MAVs is endurance, which is further degraded by low-efficiency aerodynamic characteristics resulting from low Reynolds number flight. These vehicles utilize propellers significantly smaller than regular propeller-driven aircraft. The small rotational velocities and chord lengths of these propellers mean that they operate at Reynolds numbers between 5,000 and 300,000. This is far smaller than that of full-scale propellers for which $Re \geq 1{,}5000{,}000$ is commonplace. Consequently, the procedures of full-scale propeller design may have limited relevance when applied to MAVs, with the result that scaling performance values from larger propellers will be inaccurate. By the 1980s it was well known that the laminar boundary-layer separation caused rapid performance deterioration in airfoils designed for $Re > 500{,}000$ as the chord Reynolds number decreases below this point (1 p. 42). The performance of 3D wings is even less than that of airfoils. The aim of this study is to investigate some propeller design variables, such as geometric pitch distribution, airfoil type, chord length, thickness, blade loading, and solidity, and compare them over a range of advance ratios in order to find optimal configurations. Very little data exists for small propellers with diameters of 5-10cm (1), and it is possible that unconventional designs providing maximum thrust and efficiency may exist which differ significantly from conventional propeller designs. These designs may include propellers which more closely resemble electronics cooling fans and ship propellers rather than the blades found on turboprop engines, and the use of ducted propellers. These designs are beyond the scope of the study, which will look at conventional propeller geometries. The investigation will be conducted in three parts: first a literature review covering the project design requirements, the history and development of micro-air vehicles, low-Re flow, and propeller design theory will be completed. Secondly, 2D computational fluid dynamics (CFD) analyses of airfoil performance in low-Re flow will be undertaken in order to generate an optimum airfoil shape for the propeller model. Finally, 3D propeller CFD simulations with varying geometric and aerodynamic properties will be undertaken and compared to thrust and torque outputs generated using Jan Roskam's method of prediction of in-flight thrust and power (3).

II. Micro-Air Vehicles (MAVs)

A. MAVs and Propulsion Systems

In 1992 the Defence Advanced Research Projects Agency (DARPA) began considering a wide variety of devices for defence applications, one of which was flying vehicles with a 1cm span. After feasibility studies, which acknowledged the limitations of the technology of the day, interest turned to developing aircraft with a 6-inch (15.25cm) maximum dimension, which would be capable of carrying electronic detection and surveillance sensors. And so the development of the micro-air vehicle began (1).

MAV propulsion systems are normally propeller driven and powered by DC electric or small internal combustion engines. A popular choice for larger MAVs is the COX TEE-DEE .01 internal combustion engine where the thrust requirement is around 1N (4). However, for smaller aircraft, the electric motor is the ideal choice. Because of their small size, MAV performance is sensitive to small weight changes and propulsion systems must be as small, lightweight and efficient as possible. For a 0.15m wingspan MAV, a fixed-wing, electric-motor, prop-driven system is the most efficient (1 p. 67). The major limitation of battery propulsion systems is their low energy density; however, the development of batteries is still making significant advancements such that possible flight endurance times are periodically increasing. Most DC motors have an electrical to mechanical conversion efficiency of 50-75%, and brushless DC motors, such as the example shown in fig.1, have recently

Figure 1. Brushless DC motor for model aircraft. (46)

become very popular with model aircraft operators due to their high efficiency and light weight. An example of such a motor is the A-10S Brushless Motor, which has a maximum RPM of 25,000 and a weight of only 15g (5). Further details of the A-10s can be found in appendix A. The power required by the MAV propeller will depend on the torque and RPM at which the propeller operates, and engine selection will have to take into consideration the propeller efficiency and engine efficiency. Typically, the sum of the power required for propulsion, controls and payload is between 2-10W (1). In designing, fabricating and testing entire MAV designs, Mueller et al. (1) found that propeller sizes were limited by stability and efficiency. For small single-propeller aircraft, propeller diameters greater than one-half the wing span would result in difficulty in countering propeller torque and slipstream effects; however, below a propeller diameter of three inches high efficiency could not be attained. Where the propeller diameter is less than three inches, flapping wing designs emerge as the most efficient means of propulsion.

B. Benchmark Review

The following benchmark review has been completed to compare recent MAVs that have been employed or designed for military purposes. Data has been collected from Janes Online Database (6) for the AeroVironment Wasp and Wasp III, AV Black Widow, AV Hornet, MicroSTAR, CASIC LT, Honeywell RQ-16A T-Hawk, EADS DS Do-MAV and from other sources for the ARA NightHawk (7) (8), Barnhart et al.'s MAV1 and MAV2 (4) and Mueller et al.'s MITE3 and MITE4 concepts (1). The data collected will allow a statistical estimation of the expected weight and endurance of a MAV given a certain wingspan. The review has been summarized in Table 1.

Model	$W_{to\ max}$ (g)	b_{wing} (m)	End. (min)	Propulsion	Launch	V_{cr} (kts)
Barnhart MAV2	33	0.12	15	2-blade tractor prop	Hand	21
Barnhart MAV1	43	0.14	15	2-blade tractor prop	Hand	27
AV Black Widow	80	0.15	22	Lithium electric, 2-blade prop	Pneumatic	23
MITE3	129	0.25	-	Electric lithium polymer battery, dual 2-blade prop	Hand	19
BAE MicroSTAR	142	0.15	20+	10W electric, lithium batteries, 2-blade prop	Hand	30
AV Wasp	170	0.33	40-70	Electric, lithium-ion polymer battery (9W), 2 blade prop	Hand	20-35
AV Hornet	170	0.38	5	9W+ electric, hydrogen fuel cell, 2-blade prop	Hand	-
MITE4	230	0.47	25	Coreless DC electric motor with dual 2-blade prop	Hand	19
AV Wasp III	430	0.72	45	Electric, 2-blade tractor prop	Slingshot	35
EADS DS Do-MAV	500	0.42	30+	Battery-powered electric, two-blade pusher prop	Hand	-
ARA NightHawk	725	0.66	70-90	Electric lithium polymer battery, 2-blade prop	Hand	18-35
CASIC LT (A)	-	0.22	20	2-blade tractor prop	Hand/bungee	38
Honeywell T-Hawk	7800	0.56	50+	Flat twin piston, fixed-pitch ducted fan	VTOL	50

Table 1. Comparison of Contemporary MAVs.

C. Statistical Analysis of Design Points

The data gathered in Table 1 assist in approximating the size and flight speed of the MAV design. The Honeywell T-Hawk data has been included as an example of a VTOL MAV; however, should not be used as a benchmark for correlating mass and forward speed for a fixed-wing design as the wingspan value listed above for this platform is in fact its height. Of particular interest are the BAE MicroSTAR and AV Black Widow, shown in figures 2 and 3 respectively, which have identical wingspans to the project requirement. According to Mueller et al. the Black Widow is one of the smallest and most successful MAV configurations, and can carry a colour video camera and a transmitter (1). Its gross

Figure 2. BAE MicroSTAR MAV

weight amounts to 80g and depending on the literature consulted, the MAV is reported to be propelled by a 2.67-4.00in. (6.78-10.16cm) propeller (1) (9) and powered by a 10W DC motor. Even though these two benchmark MAVs have respective weights of 80g and 142g, the project will focus on designing a propeller for a 150g MAV. A goal weight of 150g allows for design flexibility should the 0.15m platform exceed the weight trends of these commercial MAVs, and may also mean that additional payload could be carried.

A numerical study was completed to examine the sensitivity of the propeller advance ratio to forward flight speed and propeller RPM, as advance ratio also equates to a given angle of attack at a propeller radial station. Propeller advance ratio is defined as:

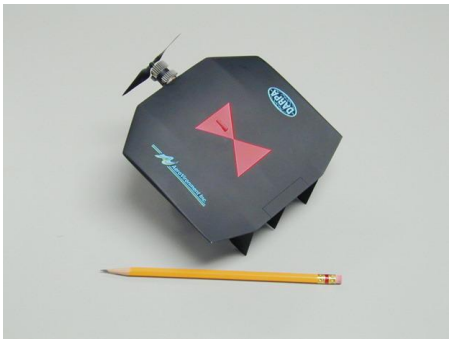

Figure 3. AV Black Widow MAV. (6)

$$J = \frac{V_a}{nD} \qquad \text{Eq. [1]}$$

At 20,000RPM, changes in forward speed of the MAV do not greatly alter the advance ratio as the rotational velocity is dominant. Furthermore, at high rotational speeds the propeller will better maintain the lift generating regions of the propeller blades in favourable Reynolds number regions, improving efficiency. A lower design flight speed means that the advance ratio will change less with changing RPM, and give the MAV pilot greater controllability if it is being directed through a remote-control system. The results from this study indicate that the propeller angle of attack should be least sensitive to small changes in forward flight speed and propeller RPM at high RPM and low V_a values. The generated charts from this advance ratio sensitivity study can be found in appendix B. and In an annual MAV design competition held at the University of Florida, MAV designs flew on average at 11.2m/s with lift coefficients of 0.42-0.52 (1). In comparison, the Black Widow is reported to fly at a forward speed of 11.8m/s, the AV Wasp flies at speeds as low as 11.2m/s. Hence the design forward speed for the propeller speed, known in propeller design as the speed of advance or advance velocity (V_a), can be justifiably set at 11m/s, and the propeller RPM will be 20,000RPM, which is within the operating range of many small electric motors.

III. Design Requirements

A. Fundamental Requirements

The propeller will be designed for a MAV weighing 150g with wingspan of 150mm and a loiter speed of 21.4kts (11m/s or M = 0.032 at 100 ft) operating at 20,000RPM. The engine power rating will be determined by the propeller torque, RPM, and motor efficiency. By designing the propeller for the higher weight requirements, the propulsion system may allow the SEIT MAV to carry heavier payloads. Using these requirements, a thrust estimate analysis was undertaken for three cases, including two cases of level flight in the loiter condition and one case in a 10° climb condition. The associated calculations for the thrust estimate can be found in appendix C. The thrust estimates were based on a flying wing layout, a scaled conventional propeller aircraft layout and finally a wing with an aspect ratio equal to one, at a 10° climb angle. The thrust requirement estimated for level constant velocity flight varied significantly between 0.046-0.340N and the required thrust for 10° climb was 0.7N. As a reference, the Black Widow, at a mass of 80g, had a thrust requirement for level constant velocity flight of 0.09N. A reasonable thrust design point for the MAV propeller will be 0.24N, which is closer to the maximum estimate for level flight, as the thrust require for climb was significantly greater than the other estimates. The required engine power rating for the climb and level flight conditions, for a weight of 1.47N (150g) is 12.47W and 6.09W respectively, which falls within the expected values for a MAV. A summary of the MAV design requirements is shown in table 2.

Propeller/MAV requirement	Value	Importance	Notes
Level flight thrust	0.24N	Essential	MAV cannot fly without this minimum thrust produced
10° climb thrust	0.7N	Desirable	Desired climb angle, can climb at smaller angle if requirement not attained
Efficiency	$\eta_p > 0.5$	Essential	If not exceeded, COTS propellers will provide similar efficiencies
Diameter	5-10cm	Essential	Failure to comply with limitations can result in significant efficiency or stability problems
RPM	20,000	Desirable	Flexible requirement but optimal for minimum advance ratio sensitivity to changes in advance velocity
Advance velocity	11m/s	Desirable	Flexible requirement but optimal for minimum advance ratio sensitivity to changes in propeller RPM

Table 2. Summary of project design requirements.

B. Project Planning

The initial scope of this project was to test a number of manufactured and commercial off the shelf model propellers in a wind tunnel to determine a design that is suitable for use on an MAV platform. It was later decided that the testing methodology would focus on CFD simulations rather than wind tunnel testing, which meant that the initial project planning documentation became largely irrelevant. For reference, the planning documentation can be found in appendix D.

IV. Propeller Theory and the Effect of Low Reynolds Number Flow

One of the significant milestones in the history of flight was the achievement of powered flight by the Wright brothers in 1903. Their achievement was made possible largely by their effective propeller design. After realising that contemporary ship propeller design was based on empirical methods, the brothers combined existing momentum and blade element theories to design a propeller suitable to propel their Wright flyer (10). The following sections will give a brief overview of propeller theories including momentum theory, blade element theory and some propeller design methodologies found in literature, followed by information pertaining to low-Re aerodynamics.

A. Momentum Theory

The following section is based on momentum theory of propellers for propeller blades with an aerofoil shape. The lift produced by a propeller depends on engine RPM, propeller airfoil shape, blade angle of attack and aircraft speed (11 p. 13) Because each blade section travels at a different speed, it may be possible to ascertain the optimum pitch distribution and airfoil thickness distribution through computational fluid dynamics (CFD) and eventually wind tunnel testing. However, this optimisation is only possible if the propeller efficiency is adequately sensitive to changes in pitch distribution and airfoil thickness.

1. *Thrust Calculation*

The thrust generated by a propeller depends on the volume of air accelerated per unit time, and on the density of the air (12). Based on momentum theory, this can be expressed as:

$$T = \frac{\pi}{4} D^2 \left(V_0 + \frac{\Delta V}{2}\right) \rho \Delta V \qquad \text{Eq. [2]}$$

Where ΔV is the change in velocity of the air as it passes through the arc of the propeller.

2. *Power*

Power is defined as force multiplied by velocity. The propulsive or available power of a propeller is defined as the available thrust T multiplied by the aircraft's velocity (or freestream air velocity).

$$P_a = Tv \qquad \text{Eq. [3]}$$

3. *Efficiency*

Efficiency (η) relates how much thrust we are achieving from the propeller for a given engine power, and is the ratio of P_a to the engine power P_{engine} :

$$\eta = \frac{P_a}{P_{engine}} = \frac{Tv}{P_{engine}}$$ Eq. [4]

According to Hepperle (12), for a given power P, it is desirable to use the largest possible propeller diameter. In most cases this is restricted by landing gear height, fuselage clearance, tip Mach number or other mechanical/aerodynamic considerations, however these restrictions apply to a lesser extent in the case of a MAV and are worthy of further investigation. The relationship between forward velocity, propeller diameter and propeller efficiency is given by the following relationship:

$$v = \eta \left(\frac{2P}{\pi \rho D^2 (1-\eta)} \right)^{1/3}$$ Eq. [5]

This relationship is shown graphically in Figure 4. Since v =11m/s for the MAV and the estimated $\frac{P}{D^2} = \frac{6.09}{0.08^2} = 951.6$, the approximate attainable propeller efficiency for a MAV is 82% at sea level. However this applies to full-scale propellers and is an 'ideal' result, and results may differ for flows with Reynolds numbers of the order encountered in MAV flight. Hepperle does suggest that real world propellers only achieve 0.8 of this ideal efficiency, meaning the actual achieved efficiency will be closer to 66%. If rotational losses due to the swirl of the airflow behind a propeller are also taken into account, a further two to five percent efficiency is lost (12).

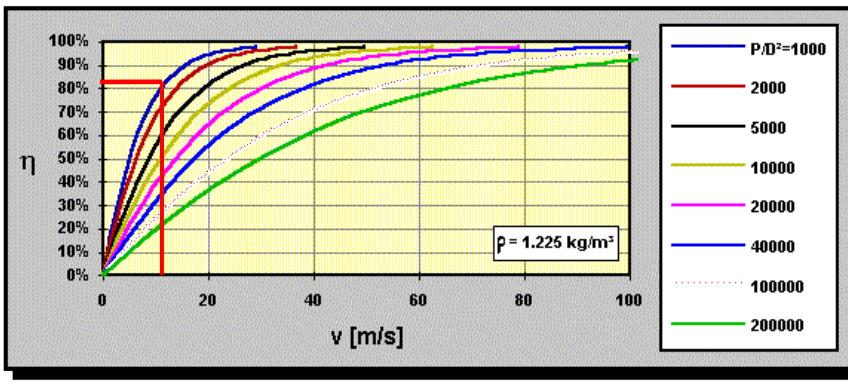

Figure 4. Relationship for ideal propeller efficiency vs forward speed (12)

Barnhart et al. (4) found that although the published propeller efficiency achieved by the Black Widow was 78%, for the four MAVs tested in their report, the propeller efficiency ranged between 33-75% and that most off-the-shelf propellers had an efficiency of 40%. The report *Development of the Black Widow Micro Air Vehicle* (9) reveals that there were in fact two propellers used in the development of the Black Widow, a 2.67in. $\eta_p = 63\%$ direct drive propeller, and a 3.81in. $\eta_p = 80\%$ geared prop with a gearbox efficiency of 81%.

4. Limitations

Momentum theory does not take into account factors such as the planform of the blade nor the characteristics of the propeller airfoil, but does allow a good approximation of the maximum expected efficiency of a propeller. It also allows the deduction of the effects of flight speed, air density and propeller diameter on thrust, power and efficiency. However for more accurate analysis, Blade Element (BE) Theory must be used.

B. Blade Element Theory (BET)

BET is a numerical method of calculating the performance of propellers and rotors, performed by dividing the length of the blade into strips of width *dr*. Each *dr* section is moving at a rotational velocity of $2\pi nr$, where n is the propeller rotational velocity in revolutions per second. The net velocity component also has a forward velocity, V, or advance velocity. Each *dr* segment has lift (dL) and drag (dD) forces acting upon it, with dL acting perpendicular to the vector sum of V and $2\pi nr$, while dD acts along but opposite to

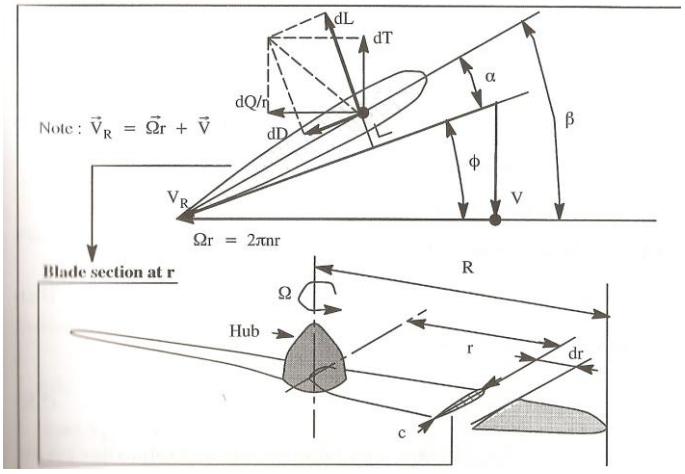

Figure 5. Geometry of a propeller blade element (3)

that vector sum. The force element *dT* is the element thrust, and the force element perpendicular to *dT* is the force contributing to the propeller torque, equal to *dQ/r*. Both *dT* and *dQ* can be calculated and integrated over the span of the blade and the entire propeller (accounting for number of blades) to give the total thrust and torque. However, the sectional aerodynamic characteristics of each blade element, affected by the local induced velocity due to lift production, must be known before this can be done so accurately (13). This can be done by combining momentum and blade element theory into combined blade-element and momentum theory (BEMT). The *L/D* of a propeller airfoil can be directly related to the propeller T/Q ratio, which is proportional to propeller efficiency. According to propeller theory $dT = dLcos\phi - dDsin\phi$ and $dQ = (dLsin\phi - dDcos\phi)r$ (3) where ϕ is the helix angle Furthermore:

$$\eta_p = \frac{P_a}{P_{shaft}} = \frac{Tv}{P_{shaft}} \quad \text{Eq. [6]}$$

$$P_{shaft} = 2\pi nQ \quad \text{Eq. [7]}$$

$$\eta_p = \frac{Tv}{P_{shaft}} = \frac{Tv}{2\pi nQ} \quad \text{Eq. [8]}$$

$$\eta_p \propto \frac{T}{Q} \quad \text{Eq. [9]}$$

C. Low-Re Flow Aerodynamics

One of the main issues limiting the performance of MAVs is the degraded performance of airfoils and propellers at small scale. Bohorquez et al. (14) observed that when designing rotors for MAV-sized helicopters, the scaled-down rotors experienced blade efficiencies between 0.3 to 0.6, compared to the figures of merit of around 0.8 attained by full-scale helicopters. For helicopters, values of Re less than one million were considered 'small' historically, however with the advent of UAVs, small research prototypes with rotor diameters between 18 and 23cm and masses of 200-400g operate in Re in the range of 30,00 to 60,000. Merchant (15), in testing propellers with diameters between 6-22 inches, found the chord-Reynolds number ranged between 30,000 and 300,000, and found that the low-Re effects began to significantly alter performance as the lower value was approached. An estimation of the Reynolds number at the 0.75r point of the propeller for the project MAV can be made, assuming an RPM of 20,000, mean aerodynamic chord of 5mm and diameter of 80mm, at an air temperature of 300K at sea level:

$$V = \omega . 2\pi r = 62.83 m/s \quad \text{Eq. [10]}$$

$$Re = \frac{\rho VD}{\mu} = \frac{1.225 \times 62.83 \times 0.005}{1.983 \times 10^{-5}} = 19{,}406 \quad \text{Eq. [11]}$$

In this example, the effect of the forward velocity of the MAV has been ignored, but the Re is of the order of 20,000, which falls within the *Re* range affected by the laminar boundary layer separation. As Reynolds number reduces, viscous forces become dominant, resulting in boundary layer behaviour different from that found in larger airfoils. Carmichael (16) in his report 'Low Reynolds Number Airfoil Survey,' identified distinct aerodynamic regimes within Reynolds numbers of 5,000-60,000, the first grouping of which is extended by Bohorquez et al. (14) to 1,000-10,000 and hence incorporates the inner radial sections of the MAV propeller. This regime is characterized by laminar flow which tends to separate before undergoing transition, which will adversely affect efficiency, and it is mentioned that computational results indicate that airfoil design, particularly camber distribution, is an important factor in determining the airfoil performance. The second regime of 10,000-30,000 has very similar characteristics to the first (14). According to Mueller et al. the choice of airfoil section operating in this Re-regime is very important, because for even up to $Re = 50{,}000$, the free shear layer after laminar separation does not normally transition to turbulent flow in time to reattach to the airfoil surface, instead forming a laminar separation bubble as seen in fig. 5, which can cause complete airfoil stall when the bubble extends to the leading edge, resulting in large increases in drag and a sharp decrease in lift. This behaviour was recorded by the 2D airfoil simulations at high angles of attack as shown in figure 6.

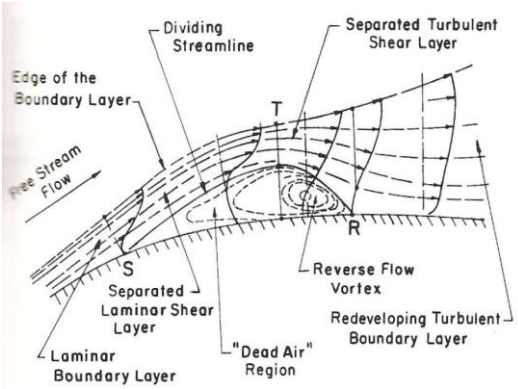

Figure 5. Time averaged features of a transitional separation bubble. (1)

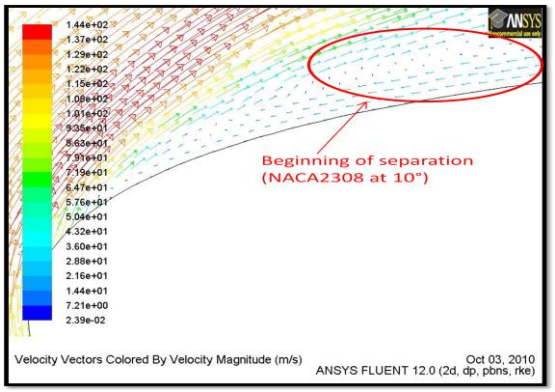

Figure 6. Laminar separation bubble as recorded in 2D CFD simulations.

Carmichael's data notes that this laminar separation bubble is a significant problem for flows in the region of $30{,}000 \leq Re \leq 70{,}000$, and introduces hysteresis in experimental measurements. Thick airfoils (t/c > 6%) in low-Re flow tend to experience significant hysteresis in the lift and drag forces caused by the laminar-turbulent transition, however thinner airfoils tend to have low stall angles, such that airfoil thickness selection is a compromise. In designing propeller blades for low-Re flow, minimisation of airfoil shear drag is desired in a similar manner to full-scale designs (14). This implies minimising the blade regions which are experiencing separated flow, either by increasing the chord Reynolds number over the radial blade sections (through increasing chord or rotational speed) or by inducing turbulent flow through use of leading edge turbulators and boundary layer trips. The later option becomes more effective as the Reynolds number approaches 50,000. For $Re > 70{,}000$, laminar-turbulent transition generally occurs without separation; however, this is entering the flow regimes of fixed wing RC models and other aircraft larger than MAVs. Even in this region, reducing Reynolds number has negative effects on propeller efficiency, as demonstrated in figure 7.

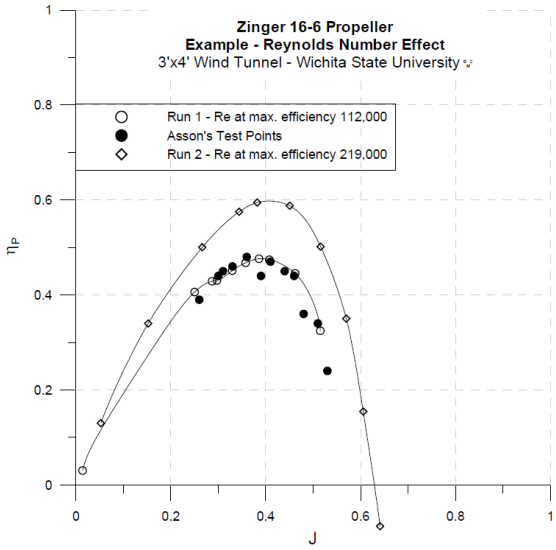

Figure 7. Effect of Reynolds Number on Efficiency.

D. Fundamentals of Propeller Design

Propeller design involves coordinating a large number of variables. Historically, propellers are designed to satisfy requirements pertaining to take-off performance, cruise performance, climb performance, maximum speed capability and FAR 36 noise requirements (3). Furthermore, propeller design is usually specific to a given engine, which delivers a known horsepower at a known RPM for a known aircraft forward speed (17). The design process adopted for the MAV propeller differs, in that a thrust requirement is given, with certain diameter limitations, and the aim is to produce the most efficient propeller. The propeller RPM and advance velocity determine the helix angle, the lift coefficient of radial element sections determine the inflow distribution, correct selection of thickness and airfoil type is necessary for good efficiency. Diameter, pitch and blade activity factor must be properly selected to draw the correct power from the engine, to ensure that propeller overspeed does not occur. All sources recommend that a propeller diameter should be selected large as possible to maximise efficiency; however, as previously mentioned, this is often limited by issues of ground and fuselage clearance and tip Mach number. A larger diameter for the same thrust requirement will allow use of a higher aspect ratio blade, which increases aerodynamic performance, at least for full-scale Re regimes. To maximise airfoil performance, the radial blade sections should be operating at an angle of attack for maximum *L/D* (18), and ideally, each radial section should use an airfoil section that gives the maximum possible *L/D* (19). For fixed-pitch propellers, if greater off-design efficiency is desired, it is recommended to use a lower blade angle of attack so that stall does not occur for flight regimes with low advance velocities. The use of propellers operating in low advance ratio regimes offers the advantage that even at very low advance velocities, it is unlikely that the blade sections will reach stall angle. The most commonly used blade airfoil sections are the RAF-6, Clark-Y and NACA-16 series (3). The RAF-6

has a high camber, which gives good take-off thrust. The Clark Y is a moderate camber airfoil with low minimum drag properties. Due to their simple design and abundance of online coordinate generators, NACA 4-series airfoils were selected for testing in the CFD simulations, where camber position, percentage and thickness could be easily varied. Thickness, and radial thickness distribution, are also important variables to be considered in propeller design, as at high angles of attack and towards the propeller hub, thicker airfoil sections are the most efficient, with a gradual reduction in thickness to the propeller tip usually giving the highest efficiencies (19). Low-lift at the propeller tip is generally desired to reduce wingtip vortices and to encourage uniform inflow. The website *Propellers for small UAVs* (20) strongly encourages the use of rounded or raked tip shapes, rather than leaving the propeller tip square. Although this was not adhered to in the CFD testing, it is a variable that can be tested in future studies. At the opposite end of the blade, Roskam (3) warns that large losses can occur in the hub area, which can be reduced by proper spinner design and use of efficient airfoil sections all the way to the root of the blade. This was verified by Weick (21), who found for a 10-ft propeller, a 5% improvement in efficiency was obtained when using streamlined airfoil sections in the shank area instead of cylindrical sections.

Selection of the number of blades is an important aspect of propeller design. Normally, the requirement for propellers with more than two blades arises from a need for more thrust. To address this, the options available are to increase engine RPM (which may be limited by tip Mach number, engine power and stresses), increase the propeller diameter (restrictions in ground prop clearance, fuselage clearance), increase the blade chord (reduces aspect ratio making blades less efficient) or to add more blades to increase the lifting area (thus increasing blade solidity). MAVs are not limited by any of these factors and it is usually most efficient to vary the propeller diameter according to the thrust requirement. A larger diameter increases the aspect ratio of the blades, thereby increasing the effect of airfoil tip-losses due to the vortex effect. The advantage of more propeller blades is that thrust is more evenly distributed over the propeller disk which results in a reduction in induced drag as blade loading is reduced. Increasing the number of blades has some disadvantages. These include a higher manufacture cost and complexity and, for the same generated thrust, a lower propeller diameter than the 2-bladed equivalent. Furthermore, increasing the number of blades results in the use of more slender blades, leading to a lower propeller chord-*Re*, which in turn exacerbates the flow separation witnessed in low-*Re* flow and thus increases drag and reduces effective thrust. The theory also exists that the blades of multi-bladed props spend more time in the turbulent wake of the preceding blade, due to the high rotational rate compared to forward velocity, and that this can also adversely affect propeller efficiency. According to Roskam (3), this is the losses due to this wake interference are significant for $J < 2.0$. Thus, it is recommended the MAV propellers utilise two blades; however, variation of propeller blades and blade solidity is an option for investigation during this study.

V. Experimental Method

A. Testing Variables

To begin the design process, the effect of airfoil thickness, camber position, camber percentage and Reynolds number regime on *L/D* was investigated. This was completed using 2D CFD simulations of NACA 4-series airfoils, the point coordinates of which were generated using a free online Microsoft Excel spreadsheet (22). It was assumed that the airfoil parameters giving the highest *L/D* would also correlate to the maximum T/Q value for the 3D propeller models under the relationship derived in the BET section above. 3D propeller designs were then tested by varying airfoil type, thickness, diameter, number of blades and radial twist distribution. It was expected that the linear twist distribution derived would function to keep the blade airfoil sections in the most efficient angle of attack (around 6°) where possible. The thrust outputs for variation in diameter were used to both indicate trends in efficiency, as well as as determine a diameter that produces the required thrust for the MAV. Tests were also conducted varying the number of blades between one and four to indicate possible effects on efficiency. The geometry, meshing and CFD programs used in the design and testing of the 2D and 3D models were CATIA, ANSYS Design Modeller, ANSYS Mesher and FLUENT. Due to the small scope of the project, the process of optimisation was primarily linear; by optimising one variable, this setting was locked in (such as thickness), then the optimum performance point for the next variable was found at this thickness, and so on. The following sections will give an overview of CFD, and the methods and models used in the 2D airfoil and 3D propeller model tests.

B. Computational Fluid Dynamics

Wind-tunnel testing is a powerful tool for the analysis of aerodynamic performance; however the manufacture of propeller models is limited by time and cost constraints. Furthermore, during a wind-tunnel investigation, individual parameters cannot be so easily varied so as to ascertain which variable is responsible for changes in performance. CFD programs, however, are tools which provide a cost-effective method of investigating aerodynamic performance, and have gained significant prominence in the design process of aircraft and their components. The complete design of a MAV is not unprecedented in both the military and in industry (1), such as the MITE concept by the US Naval Research Laboratory, as seen in figure 8. CFD codes are based upon discretisation approximations of the Navier-Stokes equations (for viscous flow), which are able to adequately describe the fluid mechanics of a model, given sufficient computation time and the correct choice of settings. Turbulence in flows is computed using simplified models based on statistical data (23 p. 357). Raymer reinforces that CFD does not replace the wind tunnel or necessarily reduce the test hours, however it provides a means of understanding the flow around an object, and normally has the advantage of being able to do this at full-scale. It is expected that the trends identified in this report through CFD will allow the fabrication of optimised propeller designs, and identify problems such as unwanted vortices and flow separation before verification through wind-tunnel testing.

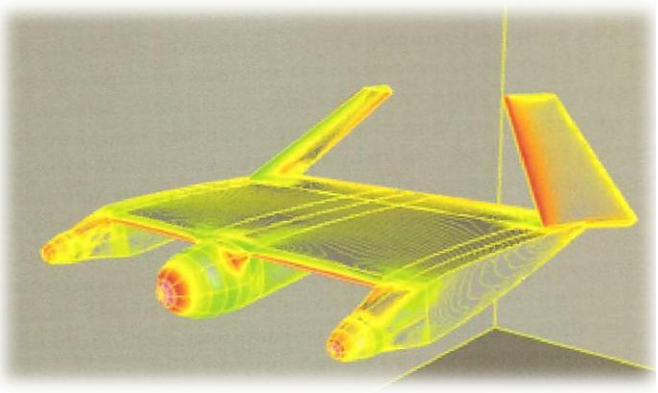

Figure 8. CFD pressure distribution on MITE MAV. (1 p. 179)

The most important parameters to consider when designing the CFD model, apart from the solid model of the propeller blade, will be the mesh applied to the model, and the turbulence model used. CFD analysis results can vary greatly with small variations in the mesh size and shaping at key points where the flow properties are changing, such as leading edges, corners and separation areas. In the case of the propeller blades, a high density of grid cells is required at the leading and trailing edges and the blade tips, with a multi-layered inflation applied to the blade surfaces. Small cell size and density is not only important for solution precision, it also affects the shape of the object 'seen' by the computational flow. A study completed by Sheng et al. (24) illustrates this loss of shape of a ship propeller when too coarse a grid is used. Even if a geometric model is formed precisely, the shape between individual points is limited by the smallest grid size, as seen in figure 9.

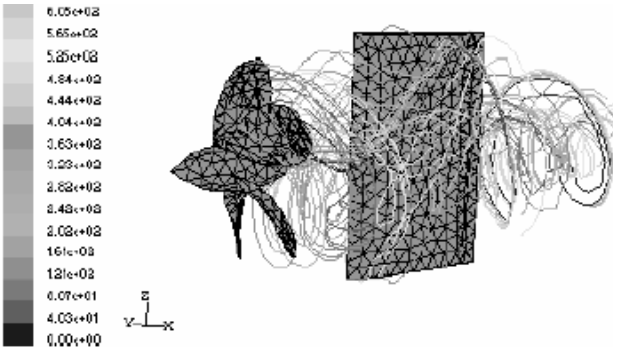

Figure 9. Loss of shape definition due to coarse mesh.

C. 2D CFD Model

2D airfoil testing was conducted to investigate the effects of thickness, angle of attack, camber position and camber percentage on lift on drag (*L/D*) and find optimum cases. The effect of low Reynolds numbers on airfoil *L/D* was also investigated. The airfoil shapes were generated in the ANSYS DM through a coordinate import system using 200 points in total, 100 on the upper airfoil surface and 100 on the lower airfoil surface. These coordinates were generated using a Microsoft Excel Spreadsheet available online (22). The coordinates were imported into DM using the

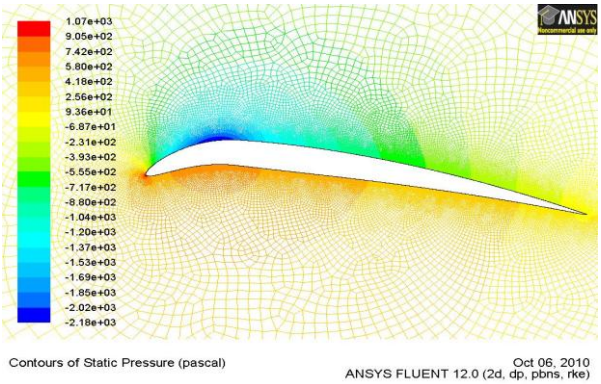

Figure 10. Pressure distribution result from 2D test for NACA7207 airfoil.

Import 3D Curve function, with all z-direction coordinates as 0.0; in order to generate a closed surface, it was important to label the final line of coordinates as zero instead of 200. After import a surface was applied to the edges of the airfoil curve. The import method was taken from page 176 of the ANSYS DM Tutorials document (25). Due to limitations of scale in DM, airfoils with chord lengths of the order of 0.01m could not be modelled smoothly, and instead produced jagged leading edges and straight line sections on the upper surface. An alternative approach was taken to import airfoils with chord lengths of the order of 1m, and then the entire geometry and mesh was scaled using the scaling function in FLUENT. A flow domain was created around the airfoil, with the airfoil positioned five chord lengths from the inlet, and five chord lengths from the upper and lower walls to ensure the airfoil was out of wing-in-ground effect. A pressure outlet was positioned 20 chord lengths behind the airfoil to ensure that pressure levels had returned to atmospheric and any turbulence had dissipated. Typically this amounted to a rectangular flow domain 10m ×26m which was scaled to 0.125m × 0.325m. The airfoil shape was subtracted from the flow domain using a *subtract* Boolean function. A hexahedral mesh was applied to the geometry with a 0.4-1mm grid sizing on the 1m chord airfoil; depending on airfoil thickness (thinner airfoils required a smaller minimum size to retain a smooth LE shape). The edge growth rate from the airfoil was 1.05. When scaled in FLUENT, this would correlate to a minimum grid size of $4.8 \times 10^{-6} - 1.2 \times 10^{5}$m, with the mesh typically containing 60-85,000 cells. The FLUENT model used was a realizable $k - \epsilon$ model with the enhanced wall treatment function applied. This model was used for both the 2D and 3D testing, as according to FLUENT v.12 Lectures (26) it is suitable for modelling low-Re flows or flows with complex near-wall phenomena such as laminar separation. The use of this model for propeller testing also has precedents; in his article *Propelling the 1903*, Christoph Hiemcke from Fluent Inc. (10) successfully modelled the propeller for the Wright Flyer using a realizable $k - \epsilon$ model with enhanced wall treatment. Furthermore, Sheng et al. (24) also used a RNG $k - \epsilon$ model to when analysing a ship propeller and rudder system, and Kulczyk et al. (27) used a $k - \epsilon$ model in their analysis of a 4119 screw propeller, and found no noticeable difference between $k - \epsilon$ and $k - \omega$. Solution methods were second order, with standard pressure treatment, and the simulations took typically 4,000 iterations and two hours for all equations to converge to residuals of 10^{-12} or lower. Where residuals reached steady state at higher residual values the result was assumed to be converged. Figure 10 is a typical pressure distribution output from the 2D testing method.

D. 3D CFD Model

The 3D testing of propeller models was undertaken to firstly confirm the trends identified in the 2D airfoil tests, and to look at propeller-specific variables such as performance for diameters between 5-10 degrees, number of blades between 1-4, twist distribution, and propeller efficiencies over a range of advance ratios.

1. Creation of 3D Propeller Geometry

The 3D propeller model comprises a spinner and two wings, assembled in CATIA. The spinner is a cylinder with a diameter of 15% of the propeller diameter, with rotated parabolic ends. Roskam (3) explains that the spinner on average forms 15% of the propeller diameter, and the parabolic ends were designed to minimise separation and drag over the surface. It was intended that the recorded propeller performance be as independent of the spinner design as possible, and in terms of thrust and torque generated, the spinner contributed typically -1.4% and 0.3% respectively.

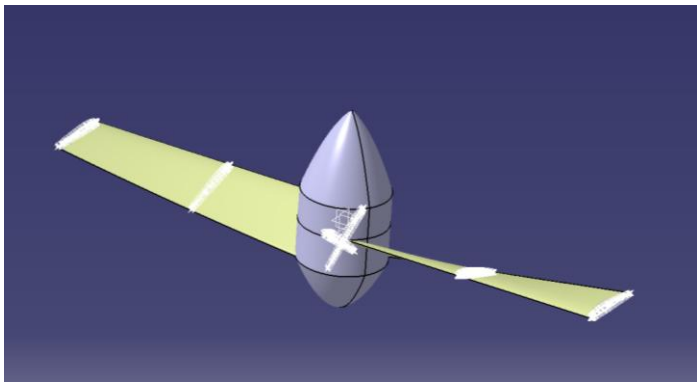

Figure 11. CATIA geometry for import into ANSYS.

The wing design was achieved by importing airfoil geometry points from Microsoft Excel into CATIA at three stations: the root, at $r = 50\%$ and the tip. An Excel spreadsheet designed by OFFCDT David Ghali for wing geometries (28), and heavily modified for propeller blade generation incorporating desired linear twist distribution, was used to generate the points at $r = 0,\ 50$ and 100%. Using an Excel macro function, the data points were imported into CATIA Part Design where lofting of the wing shape occurred and splines between the coordinates were generated, creating the propeller blades shown in fig.11. One hundred points were used to model both the upper and lower airfoil surfaces, which was particularly necessary for airfoils with high percentages of camber. CATIA was an ideal program for creating the 3D model, as it was possible to export files directly into ANSYS Design Modeller (DM) for meshing, and analysis in FLUENT, and could be used for computer-aided manufacture (CAM) of propeller prototypes in future studies.

2. *Design of Propeller Twist Distribution*

Each radial station of a propeller blade is subjected to a different incoming flow speed. The advance velocity component is constant across the blade span; however, the rotational velocity varies radially, meaning that the resultant velocity vector changes in angle to the rotation plane from root to tip. The resultant angle is known as

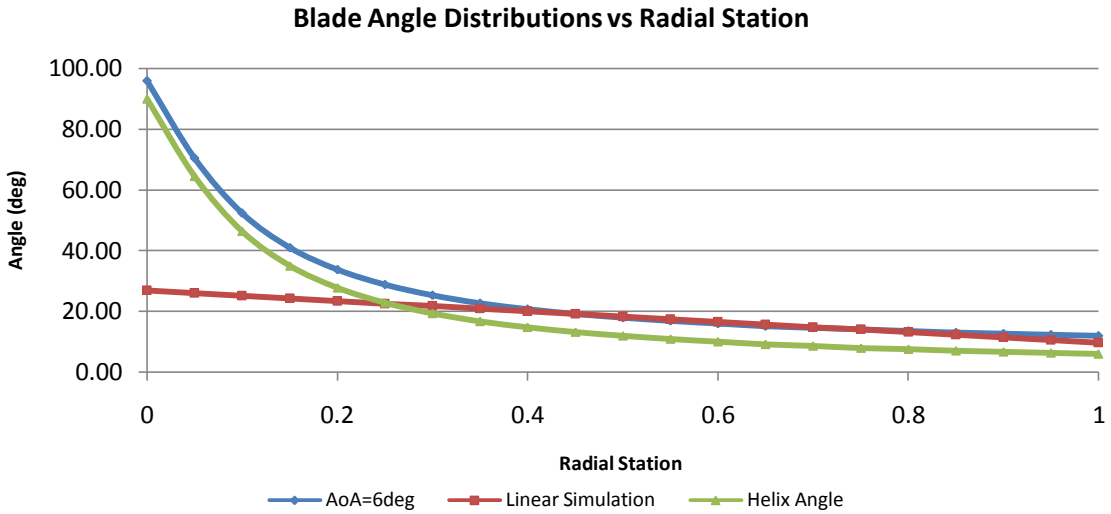

Figure 12. Linear pitch distribution for 0.1m diameter propeller designed for 20,000RPM and advance velocity of 11m/s.

the helix angle, ϕ. The angle of attack (α) of the radial blade station is defined from the helix angle, and the sum of $\phi + \alpha = \beta$, the geometric pitch angle. In this model, the induced velocity is assumed to be uniform across the span of the propeller. As the advance velocity is constant and the rotational velocity of the blade changes radially, the geometric pitch angle must be large close to the hub (where the advance velocity is dominant), and small close to the tip (where the rotational velocity is dominant). If the blade is not twisted, the local angle of attack near the hub may become highly negative, leading to a reduction in efficiency.

The design methodology for the propeller pitch distribution was based upon maintaining the 0.75r station at the optimum angle of attack for airfoil *L/D*, which was found to be 6° from the 2D testing. By setting the angle of attack at the 0.45r station 6° as well, a linear twist distribution from root to tip could be established. Figure 12 above demonstrates the linear geometric twist approximation against the geometric twist distribution required if the entire blade was to be operating at $\alpha = 6°$ for the design advance velocity of 11m/s and 20,000RPM.

For small advance ratios, the required twist along the prop is mostly linear except for the innermost radial sections. The greater the RPM, the higher the non-linearity of the twist as it approaches the hub. Thus propellers designed for higher RPMs are more suited to linear geometric pitch distributions. In the case shown in figure 12, a negative angle of attack is present until 0.26r; however this is largely covered by the spinner which occupies the blade radius until 0.15r. Furthermore, inner radial sections are not critical to lift generation being exposed to much slower flow speeds than the outer sections. It was later found that efficiency improvements could be obtained by making the blade angle of attack zero degrees at the tip, where improvements in efficiency between 0.2 to 25.9% were obtained, depending on the advance ratio for the 0.1m diameter, 2-blade NACA2307 propeller tested. It is believed that this is was due to lower lift generation at the blade tip, reducing the strength of wingtip vortices, and a higher geometric pitch angle at the hub, decreasing the negativity of the angle of attack in the inner radial sections.

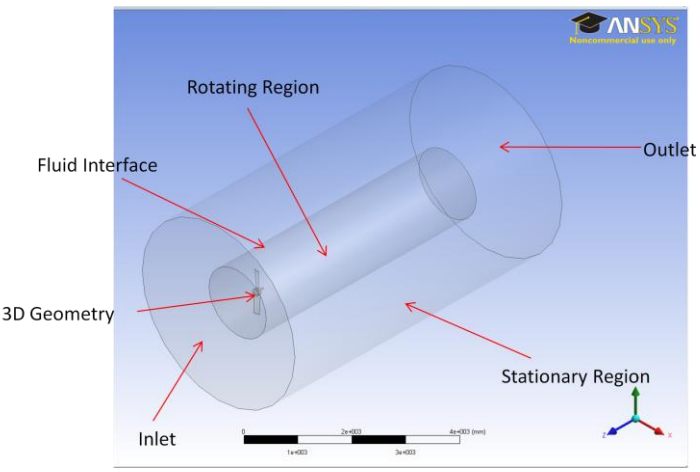

Figure 13. ANSYS DM 3D Geometry.

3. *Import into ANSYS Design Modeller*

In DM, the propeller was formed inside three cylinders in order to create the moving reference frame model required to

simulate flow around a propeller, as shown in figure 13. Many attempts were required to design a model which would function correctly in FLUENT. Figure 13 shows the correct set-up, in which the fluid interface is formed between two equally sized inner cylinders, housed inside an outside larger cylinder. Using DM Boolean subtract operations, the propeller geometry is subtracted from the first inner cylinder, forming the rotating zone; and the second inner cylinder (same dimensions as the first) is subtracted from the larger outer cylinder, forming the stationary zone. For a 0.1m diameter propeller, the inner cylinders had a diameter of 0.15m and length of 0.35m, and the outer cylinder had a diameter of 0.40m and a length of 0.7m. Dimensions were scaled accordingly for smaller propeller diameters so that mesh sizes did not become impractically large. It was found in initial model testing that even when the solution is converged, the fluid interface between the rear of the rotating region and the stationary zone did not translate the rotational component of velocity effectively. Instead, the rotating region was extended to 50% of the fluid region.

4. Meshing the 3D Model

The geometry was imported into ANSYS Mesher, where named selections were created for the inlet, outlet, blade faces, the blade tips, blade edges, spinner, both interface cylinders and the outer cylinder. A tetrahedral mesh was applied and a grid refinement was conducted to ensure that the results were adequately independent of the grid size. It was found that the critical sizing was on the blade tips and blade edges, which allowed smooth definition of the blade leading edge and adequate mesh density at the leading and trailing edges respectively. For a typical 0.1m diameter propeller, with a chord length of 0.0125m, this blade tip mesh sizing was found to be adequately small at 3×10^{-5}m and subsequent size reductions beyond this point only yielded insignificant changes in results. Further details of the grid refinement can be found in the section *3D Grid Refinement* below. A face sizing of 8mm was applied to the inner and outer cylinders forming the fluid interface, a face sizing of 0.5mm was applied to the propeller blades and an edge sizing of 0.1mm applied with a growth rate of 1.05. The fluid interface and location of the propeller geometry within the mesh can be clearly seen in fig. 14. CFX Help (29) suggests that in order to adequately model boundary layers in low-Re flow, the boundary layer should have a cell-layer 15 deep. Since the Reynolds number will change radially along a propeller blade, with thicker boundary layers close to the hub, the design point of $^3/_4\,r$ will be selected in order to assess boundary layer thickness:

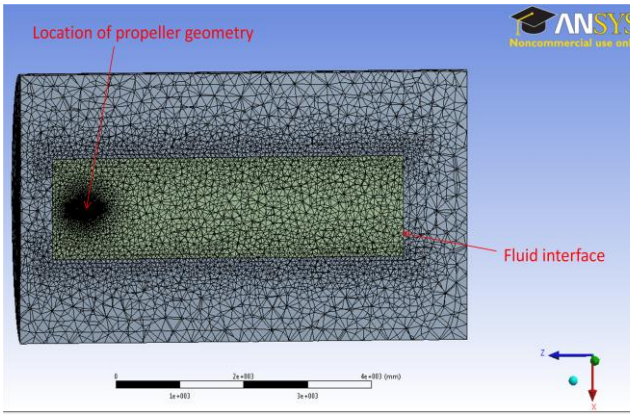

Figure 14. Section plane view of the meshed interior.

Laminar flow (30)

$$\sigma = \frac{5x}{Re^{0.5}} = \frac{5\times0.012}{58000^{0.5}} = \frac{0.06}{240.832} = 0.000249m = 0.249mm \quad \text{Eq.[12]}$$

Turbulent flow (30)

$$\sigma = \frac{0.37x}{Re^{0.2}} = \frac{0.37\times0.012}{58000^{0.2}} = \frac{0.00444}{8.968} = 0.000495 = 0.495mm \quad \text{Eq.[13]}$$

The laminar boundary layer, being the larger of the two, was selected as the design point and a 25-layer inflation was applied to the propeller blades with a maximum thickness of 0.5mm. This typically yielded y+ values over the blade of 5-6.

5. Running the Simulation

The meshed design was imported into FLUENT, where the tetrahedral mesh was converted to polyhedral grid elements. This conversion process typically took between 2-10 hours, depending on the number of elements in the original tetrahedral mesh. Conversion to a polyhedral mesh has numerous advantages, such as reducing the number of elements by up to 400%, eliminating problems of excess cell skewness (which were frequently a problem with the un-polyhedralised propeller mesh), and improved solution accuracy (31 p. 60). In some cases, using a polyhedral mesh requires half the memory and 10-25% of the computing time of tetrahedral meshes to achieve the same accuracy (32). Instead of 4-6 faces, polyhedral elements have 12-14 faces, and the higher number of surrounding elements leads to better model flows in different directions through each individual element. Polyhedral cells require more computational operations per element; however, this is offset by the reduction in total number of elements. The fluid interface was designed by assigning the two inner cylinder boundary conditions to 'interface,' and then using the FLUENT interface setup tool, creating the system displayed in fig. 15. The outlet was assigned as an outflow as the outlet airflow would not be settled only 0.6m in the wake of the propeller. Similar to the 2D model, a realizable $k-\epsilon$ model with the enhanced wall treatment model was

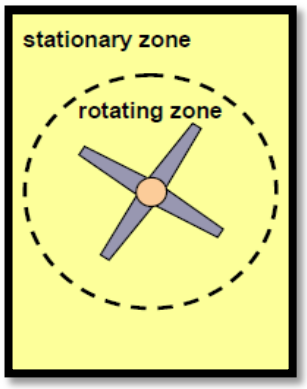

Figure 15. Moving reference frame and fluid interface concept.

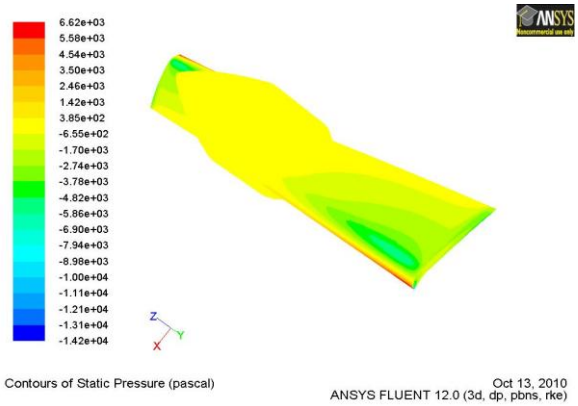

Figure 16. Contours of static pressure on a 2-bladed prop model.

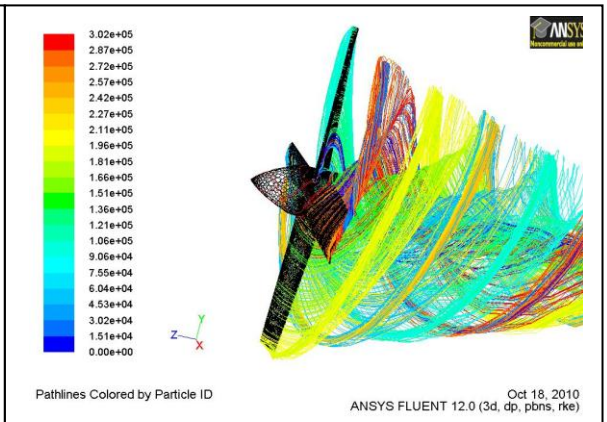

Figure 17. Pathlines from a 4-bladed prop model.

used coupled with 2nd order momentum, turbulent kinetic energy, turbulent dissipation rate and standard pressure solution methods. Air becomes compressible at flow speeds of approximately 112m/s, and the maximum tip velocity of the 0.1m diameter propeller at 20,000RPM was 104.7m/s, so the energy equation was not used. Furthermore, NASA suggests that changes in density below Mach 1.0 are very small and for subsonic flow it can be ignored (33). The rotating fluid zone as shown in fig. 15 was created by assigning the cell zone condition of the inner cylinder containing the propeller to *Moving Reference Frame*, setting the rotational reference to the z-axis and assigning a rotation speed in rad/s. All simulations were converged to residual values of 10^{-7} where possible, and where residuals reached steady state at higher values the result was assumed to be converged. This typically took between 600-800 iterations and 5-6 hours of computation time. Figures 16 and 17 show a typical static pressure distribution and depiction of flow pathlines after the solutions had converged. Checking the residuals, y+ values, pressure distributions and pathlines was important to ensure that the models were making physical sense.

VI. Results and Analysis

The following section presents results from the 2D and 3D CFD tests, an overview of the propeller optimisation process, and validation of the results using Roskam's method of in-flight thrust prediction.

A. Re effect on *L/D* (2D)

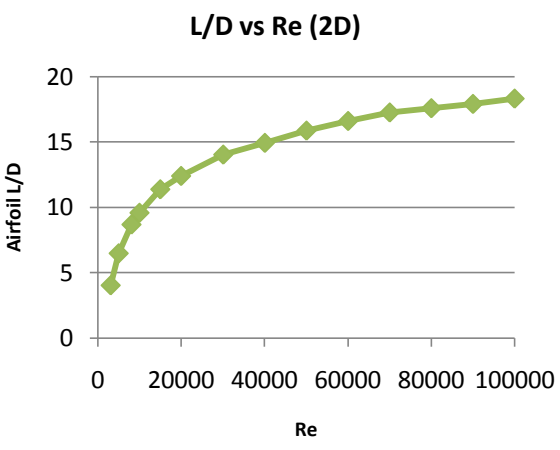

Figure 18. Effect of Reynolds Number on airfoil L/D for NACA 2308.

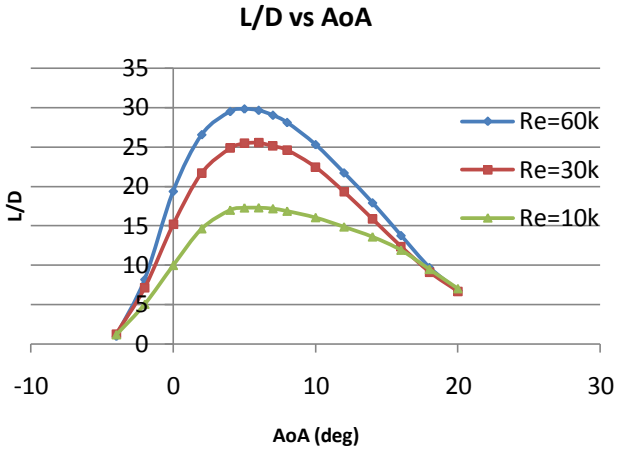

Figure 19. Effect of Reynolds number on airfoil L/D for varying angle of attack.

Figures 18, and 19 demonstrate the detrimental effect on airfoil *L/D* when operating in low Reynolds number flows. Airfoil performance markedly decreases below Re=30,000. This highlights the need to maintain the primary lift-generation regions of the propeller (around the 0.75r region) in the highest possible Re region within design limitations.

B. Optimal Airfoil Thickness (2D)

NACA23xx and NACA00x airfoils were tested at thickness to chord ratios between 1-15% and at angles of attack of 5° and 10°. The inlet velocity was set at the velocity at which the 0.75r airfoil section would be travelling for both RPM=20,000 and RPM=10,000, for a 0.1m diameter propeller. The aim of the tests was to determine whether an optimum thickness to chord ratio existed and on what parameters this optimum case depended. Results are shown below in figure 20.

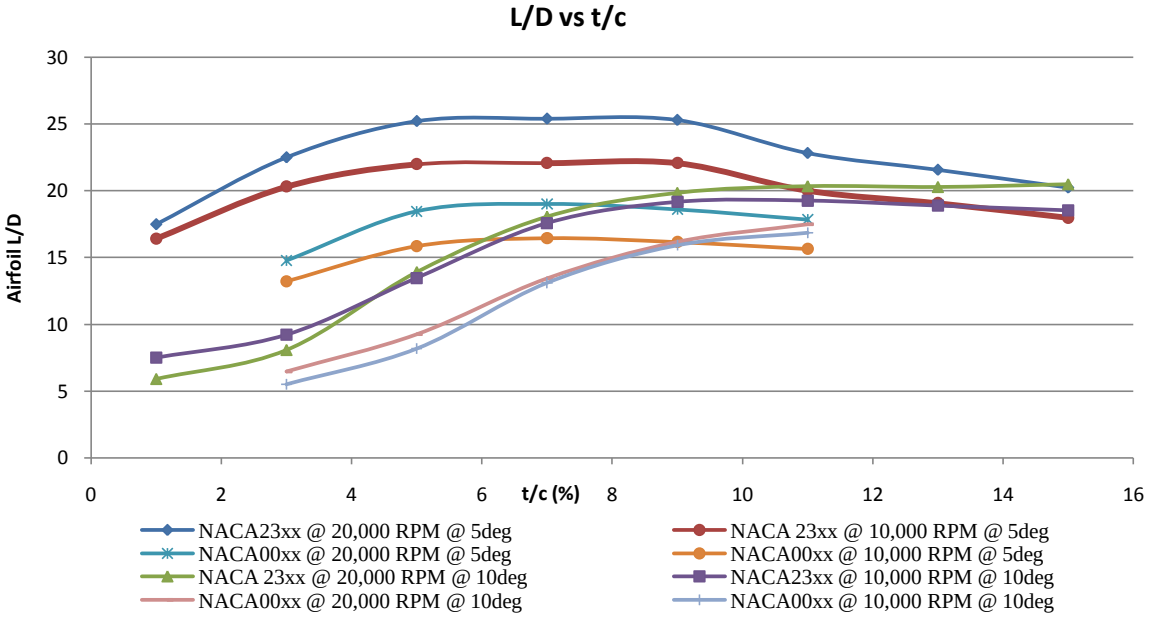

Figure 20. Variation of airfoil L/D with t/c for varying propeller RPM and airfoil angle of attack

It can be surmised that each angle of attack has an optimum airfoil *t/c*, which is independent of the airfoil type and camber, and independent of the Reynolds number regime that the airfoil is subject to. The results indicate that higher angles of attack favour a thicker airfoil, however at a lower overall *L/D*. The consequence of these results for propeller blades in which the angle of attack changes radially, is that there would also exist a radial thickness distribution to provide the highest performance over the entire blade span. Furthermore, for the same *t/c*, a cambered airfoil (NACA23xx) offers higher *L/D* performance over an un-cambered airfoil (NACA00xx).

C. Optimal Airfoil Angle of Attack (2D)

NACA23xx airfoils were tested over a range of angles of attack in order to determine the thickness and angle of attack that offered the highest *L/D* performance. The results are displayed below in figure 21. A *t/c* of 7% at 6° angle of attack yielded a maximum of *L/D*=25.43. The NACA7207 airfoil, which was the result of the 2D linear optimisation process and yielded the highest *L/D* of all the 2D tests, is shown for comparison. At an optimum angle of attack of 5°, the NACA7207 achieved a *L/D*=29.83. The thicker 11% airfoils reach a maximum *L/D* at 7°. These results indicate that for optimum propeller efficiency, the blade angle of attack should be kept between 5-7° if possible at each radial station, depending on thickness. These results are supported by a wind-tunnel study by Aki et al. (34) who found that for low-Re circular MAV wings, the highest *L/D* achieved was at $\alpha = 5°$, independent of airfoil camber and Reynolds number.

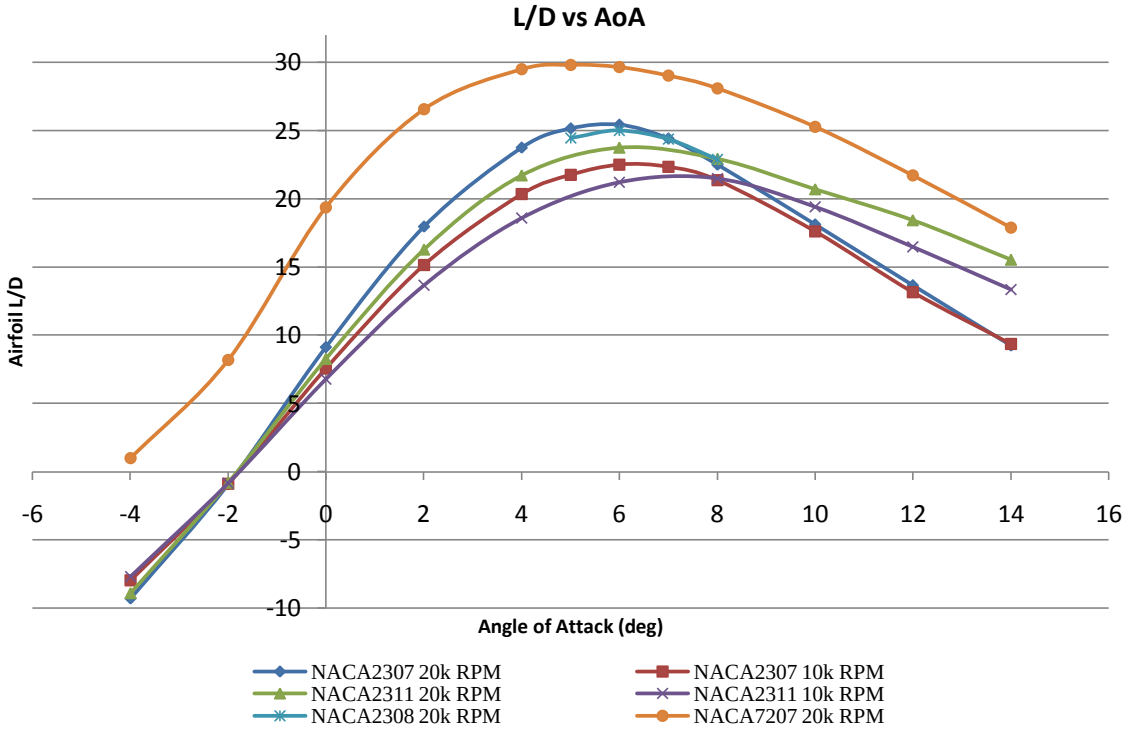

Figure 21. Variation of airfoil L/D for with angle of attack for varying t/c. NACA7207 shown for reference.

D. Optimal Camber Position and Percentage (2D)

Historically, the most common propeller airfoil blades are comprised of the RAF-6 and Clark-Y airfoils (3) . Most sections found on both ship propellers and helicopter rotor blades appear to be un-cambered NACA-4 series airfoils. The study by Sheng et al. on ship propeller performance used a NACA0009 airfoil (24) and according to Lednicer (35) the majority of helicopter rotors use NACA0011 or NACA0012 airfoils. The results in figure 21 indicate that cambered airfoils offer significant improvements in *L/D* over un-cambered airfoils.

Camber position and percentage tests were conducted for NACA2x07 and NACAx207 airfoils respectively; the latter was chosen as the camber position testing had revealed the highest *L/D* was achieved when the maximum camber was at the 0.2c position. This is displayed in figure 22. Both tests were conducted at an airfoil angle of attack of $\alpha = 5°$ with 7% thickness airfoils, consistent with the linear optimisation methodology. For both the Reynolds number regimes at 10,000RPM and 20,000RPM the 0.2c position for maximum camber yielded the highest *L/D*, however at 10,000RPM the 0.0c position yielded the minimum *L/D*, whereas for the higher *Re* regime the 0.7c position gave poorest performance.

Figure 23 illustrates the change in *L/D* with percentage camber. For the maximum camber position at 0.2c, the optimal percentage camber was 7%. This concluded the 2D airfoil optimisation testing, which indicated that a NACA7207 airfoil would be the most efficient over the Reynolds number encountered in the propeller flow. A comparison of the advantages in *L/D* performance of the NACA7207 over the other airfoils tested can be seen in fig. 21 above.

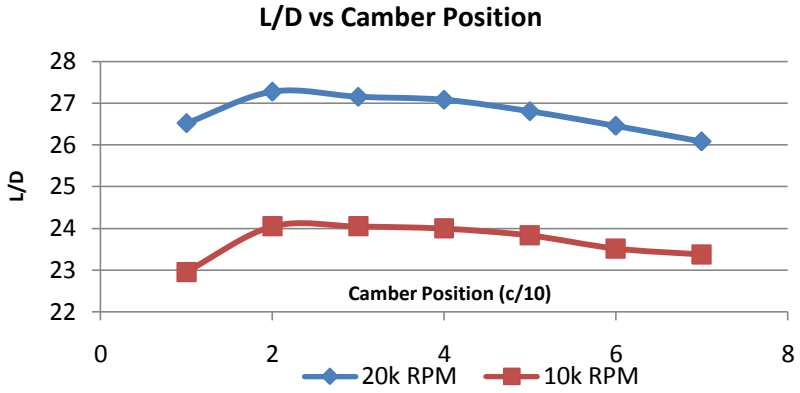

Figure 22. Variation of L/D with camber position for NACA2x07 at α =6°

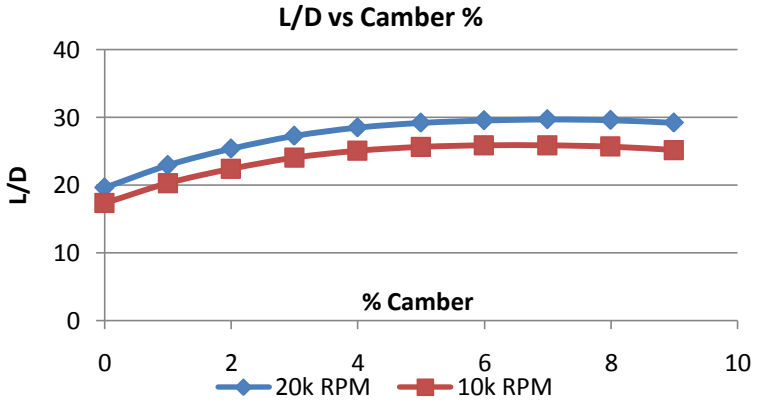

Figure 23. Variation of L/D with airfoil camber % for NACAx207 at α =6°

E. 3D Grid Refinement

Before testing a range of parameters for the 3D propeller model in FLUENT, a grid refinement study was conducted to ensure that the results were independent of the sizing of the mesh used on the propeller geometry. Often the application of a mesh is a compromise between precision and economy, as on average, a doubling in the number of mesh elements will result in an increase in computation time by a factor of ten. The aim was to find a minimum grid sizing for which smaller grid sizes would cause only insignificant changes in thrust and torque. The grid refinement study was conducted on a 0.1m propeller with a NACA7207 airfoil operating at 20,000RPM. The results of the study for T/Q are shown below in figure 24. Further grid refinement outputs, including change in thrust and torque with minimum grid size, and change in T/Q with number of total elements, can be found in appendix E. Another important assessment of mesh quality is *y+* factor, a non-dimensional wall distance for a wall-bounded flow, which indicates to what extent the mesh has allowed FLUENT to solve the boundary layer fluid mechanics. This ensures a good drag prediction and allows the turbulence model to work effectively. According to FLUENT v.12 lectures (26), when using the Enhanced Wall Treatment Option, the mesh requires high resolution near the wall, in this case the propeller surface, necessitating a y+ value < 5. With standard wall function, y+ values of 30-500 are acceptable. Examples of y+ results found in the grid refinement can be found in appendix E.

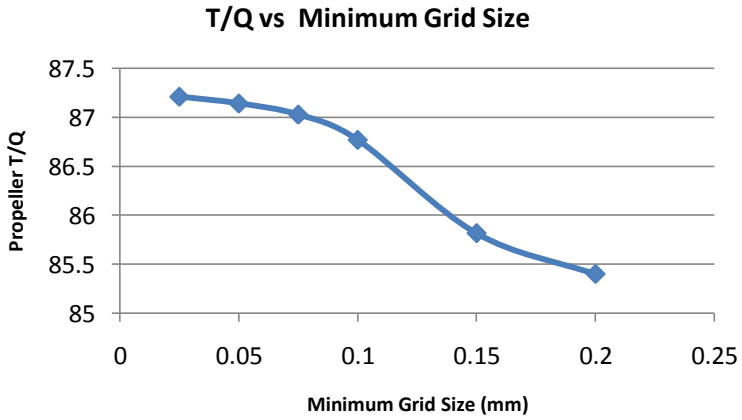

Figure 24. Grid refinement study conducted for the 3D model.

F. Re effect on T/Q and efficiency (3D)

The 0.1m diameter propeller with NACA7207 airfoil was tested at various 0.75r Reynolds numbers. This was achieved by altering the RPM and inlet speed to maintain a constant advance ratio, such that the helix angle

remained constant throughout testing. This meant that the same blade geometric pitch distribution could be used at each Re-regime. The effect of Reynolds number on propeller T/Q is shown below in figure 25.

The results match both the findings in Merchant's wind-tunnel study of low-Re airfoils (15), and the 2D airfoil data, showing a significant reduction in propeller T/Q below Reynolds numbers of 30,000, where laminar separation becomes more prevalent. These results can be compared to a similar plot for the 2D airfoil case found in appendix F.

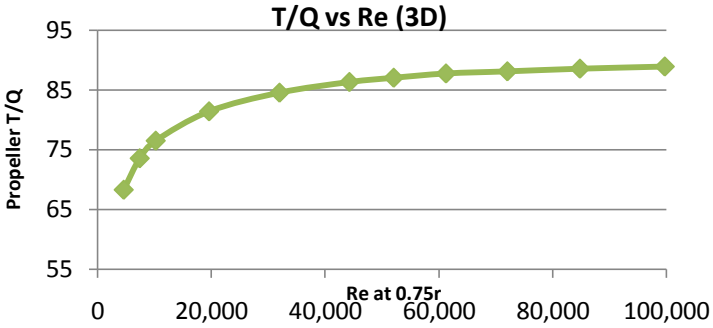

Figure 25. Effect of chord Reynolds number on T/Q for 10cm NACA7207 propeller.

G. Verification of Airfoil and Thickness Selection (3D)

The 2D airfoil testing indicated that a NACA7207 airfoil was optimal in terms of *L/D* for the Reynolds number regions encountered in the major lift generation regions of the propeller blade at 20,000RPM. To compare some fundamentally different airfoils, a zero camber airfoil (NACA0007), moderate camber airfoil (NACA2307) and the high-camber optimal 2D case (NACA7207) were used as propeller blades and tested over advance ratios of $0.20 \leq J \leq 0.84$. For the 0.1m diameter propeller used, this corresponded to a variation of inlet velocity between 5-21m/s, covering the entire possible range of MAV forward flight speeds. *J* was varied by changing the inflow velocity as this was the method used by Kulczyk et al. (27) in their analysis of a screw propeller in FLUENT. A short study was completed to verify that the same results could be obtained by varying inlet speed or propeller RPM in order to change advance ratio. The FLUENT force and torque outputs for the propeller were identical for both cases, as shown in appendix G. The results for the airfoil type testing are shown in figure 26. An advantage of examining propeller characteristics over a range of advance ratios is that performance over a range of flight speeds is known, which can be correlated to MAV flight regimes such as cruise, loiter, dive, climb and take-off.

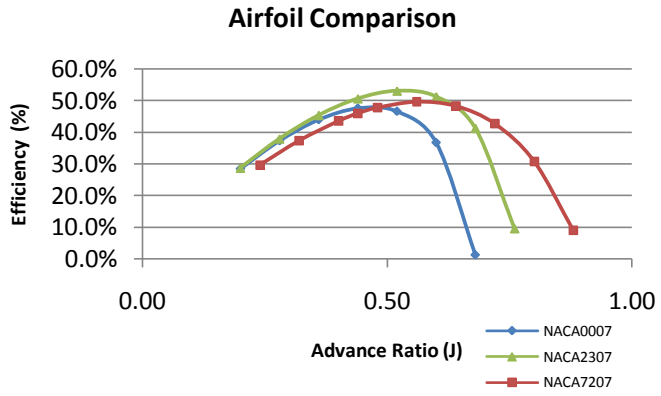

Figure 26. Efficiency of three airfoil types vs J

The results indicate that although the NACA7207 propeller was much more efficient at high advance ratios, use of a NACA2307 airfoil offered a 4.6% improvement in efficiency at the design point of 11 m/s. For the geometric pitch distribution used the NACA7207 become more efficient at an advance velocity of 16m/s. Over the entire flow regime studied, the uncambered NACA0007 airfoil offered inferior performance. It is also worth mentioning that the NACA7207 airfoil, while less efficient, generated a significant 63% greater thrust for the same blade surface area.

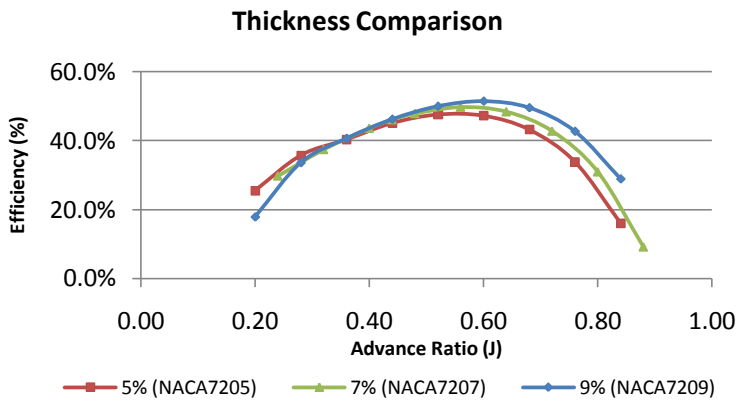

Figure 27. Efficiency of three airfoil thicknesses vs J.

A study on the effect of airfoil thickness on efficiency was also undertaken by comparing propellers

using a 5% airfoil (NACA7205), 7% airfoil (NACA7207), and a 9% airfoil (NACA7209) over a range of advance ratios. The results of the thickness study are shown in figure 27. The thickness results are also unexpected, with the 9% thickness airfoil showing a 1.2% increase in efficiency over the 7% airfoil that was found to have the best *L/D* in the 2D testing in figure 20.

H. Effect of Reducing Diameter (3D)

Using a NACA2307 airfoil and running the propeller at 20,000RPM, propellers of diameter 0.05m, 0.06m, 0.08, 0.09m and 0.1m were compared in terms of efficiency. This test was also important to determine the approximate propeller diameter that would be required to drive a MAV with a thrust requirement of 0.24N. The results are shown in figure 28.

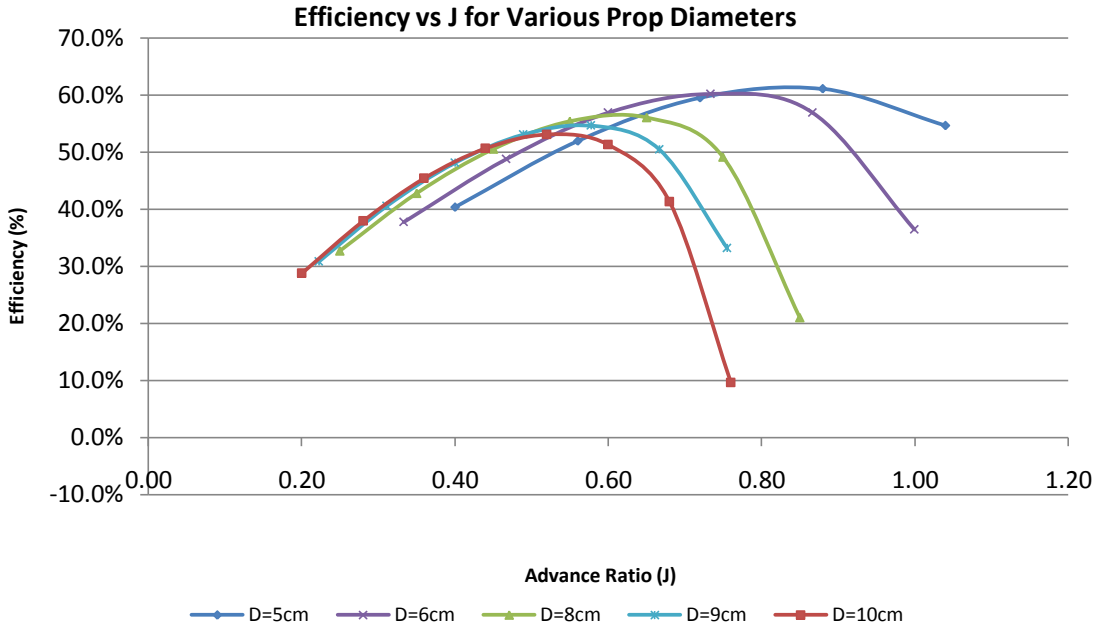

Figure 28. Efficiency vs propeller diameter over range of J.

Despite the disadvantage of operating at a lower Reynolds number regime, the lower diameter propellers demonstrated higher maximum efficiencies, and were more effective at higher advance ratios. The maximum efficiency achieved was by the 0.05m at a forward speed of 11m/s, giving 61.1% efficiency for a total produced thrust of 0.057N. An interesting comparison of efficiency vs diameter and thrust vs diameter with changing advance velocity can be found in appendix H. These charts were used to select the diameter of the recommended final propeller design.

I. Number of Propeller Blades, Blade Solidity and Blade Loading (3D)

The following study was conducted to determine the effects that the number of propeller blades (B) has on efficiency and production of thrust. Changing the number of blades directly influences the propeller solidity, and allows comparison of efficiency against blade loading. The number of blades was altered between one and four and tested over a range of advance ratios, as shown in figure 29.

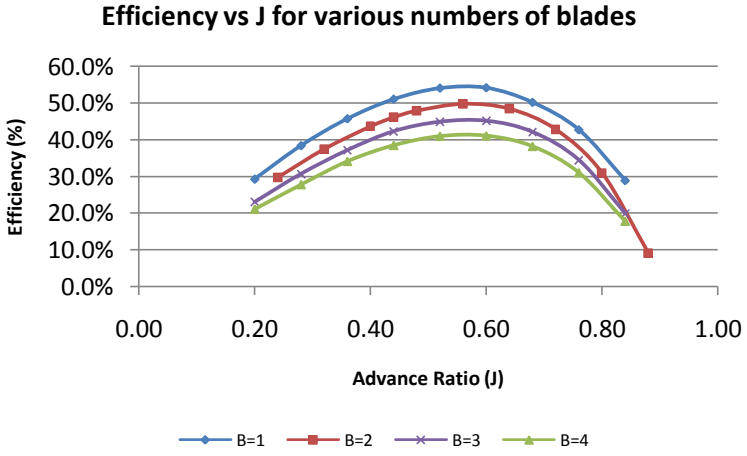

Figure 29. Efficiency for various numbers of propeller blades.

Roskam (3 p. 288) notes that at low advance ratios

($J < 2.0$) there are significant efficiency penalties for increasing the number of blades. This is due to the turbulent wake of the preceding blade having less time to settle and move downstream before the next blade enters the wake. Blade loading is defined as:

$$P_{bl} = \frac{4P}{\pi B D^2} \quad \text{Eq. [14]}$$

Propellers with high blade loadings also tend to suffer from reduced performance for $J < 2.0$ which may explain the increase in efficiency for the smaller diameter propellers. This trend can be seen in table 3 and figure 29 for changing propeller diameters and an advance velocity of 11m/s.

Figure 30 indicates that for low-Re propeller design, reducing solidity is a more important consideration than reducing blade loading. For a constant blade planform, a higher maximum efficiency is still achieved using a single propeller blade (B=1) even though it operates at a higher blade loading. This suggests that efficiency losses resulting from increasing number of blades are so great, that it offsets the advantage of reduce blade loading. It is possible that an optimum design case will involve a low number of blades, with the shortest possible diameter to deliver the required thrust.

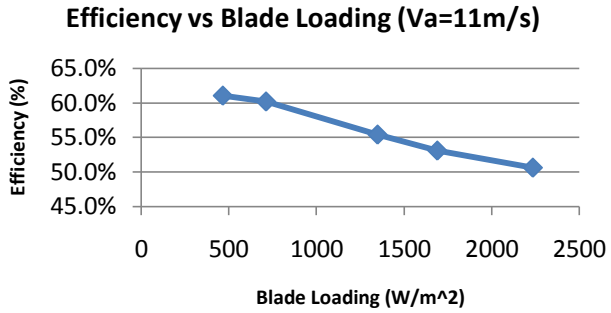

Figure 29. Efficiency vs Blade Loading

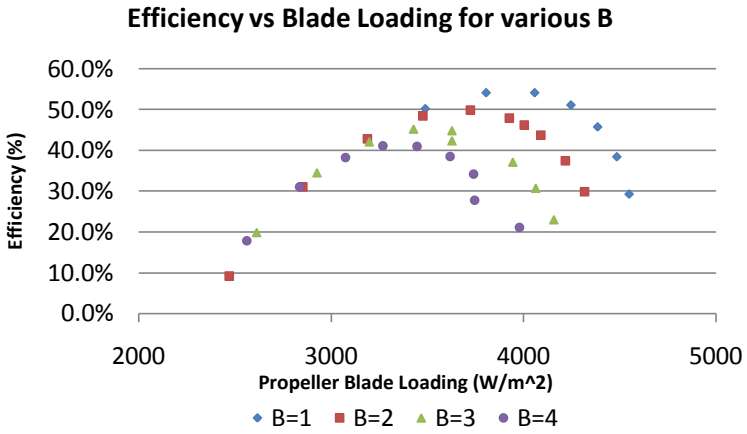

D (m)	P_{bl} (W/m^2)	η_p
0.05	464.6	61.1
0.06	711.8	60.2
0.08	1348.3	55.4
0.09	1690.1	53.1
0.10	2236.4	50.7

Table 3. Power loading and efficiency for various propeller diameters.

Figure 30. Efficiency vs Blade Loading for various numbers of blades.

J. Alternate Twist Distribution Methodology (max *L/D* over largest portion vs zero drag at tip) (3D)

Previously, tests had been conducted with propellers whose twist distributions were fitted by fixing the angle of attack at the 0.45r and 0.75r sections to 6°. This appeared to be effective, generating efficiencies up to 61.1% for a 5cm diameter propeller. To encourage more uniform thrust over the propeller disk, an alternate twist distribution method was tested using a 10cm diameter NACA2307 airfoil propeller. The alternative method involved fixing the angle of attack at the 0.75r station and blade tip to

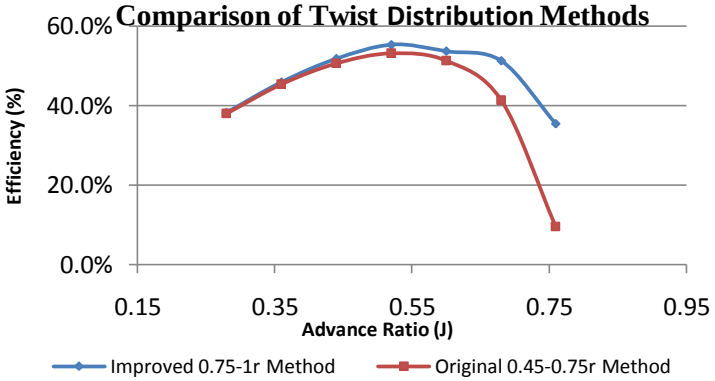

Figure 31. Comparison of pitch distribution methodologies.

$\alpha = 6°$ and $\alpha = 0°$ respectively. Using a linear approximation, the local angle of attack near the tip was reduced, and the angle of attack between the 0.35-0.6r stations increased to an average of $\alpha = 9°$. This reduction in c_l at the outer blade elements, and respective increase in the inner blade elements were expected to provide an increase in efficiency due to more uniform inflow and thrust distribution as well as reducing induced drag due to wingtip vortices. The efficiency of the two twist distribution methodologies are compared in figure 31. The improved alternative method yielded a 1.1% increase in efficiency at the design advance velocity of 11m/s, and offered significantly improved performance at higher advance ratios, rising to a 9.9% greater efficiency at $V_a = 17m/s$ and 25.9% greater efficiency at $V_a = 19m/s$ for the same NACA2307 airfoil. Various graphical outputs which describe the flow around the propeller can be found in appendix I.

K. Validation of 3D Results using Roskam in-flight Thrust Predictions

All CFD results require validation to ensure that the models are accurately calculating the flow solutions. In his book *Airplane Aerodynamics and Performance* (3), Roskam provides a process to estimate propeller thrust and power based on propeller geometric factors such as Activity Factor (AF), Integrated Lift Coefficient (C_{L_i}) number of blades (B), and mechanical and aerodynamic variables such as power coefficient, altitude, forward speed and propeller RPM. The engine power provided to the propeller was calculated from the CFD output for torque for a 0.1m diameter propeller over a range of advance ratios. The Roskam method uses propeller efficiency charts for B=3 and B=4 propellers to give estimations of in-flight thrust. For 2-bladed propellers, an extrapolation is used to estimate the free propeller efficiency using the B=3 and B=4 values. Because the power coefficients of the MAV propellers are so small (typically between 0.03-0.06), the design points often fell below the defined efficiency contours on the performance charts; in this case graphical extrapolation was used to estimate the free propeller efficiencies. An example calculation using the Roskam method can be found in appendix J. As shown in figure 32, the experimental CFD results conform well to the expected Roskam outputs for both produced thrust and efficiency.

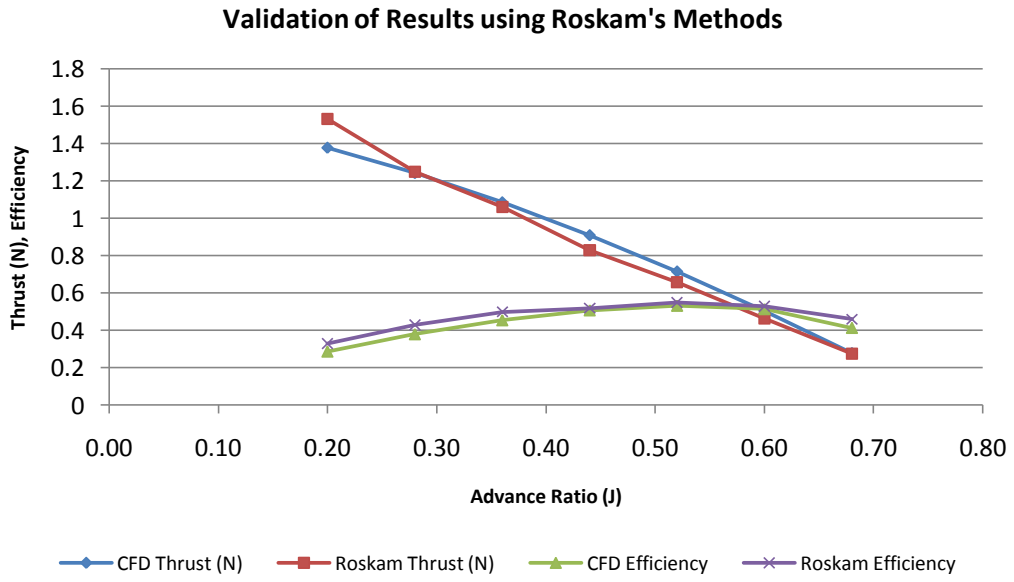

Figure 32. Validation of results using Roskam's in-flight prediction of thrust.

The propeller performance charts found in *Airplane Aerodynamics and Performance* contain the geometric pitch angles for zero angle of attack at the 0.75r station, which through extrapolation was approximately 7° for the 0.1m diameter propeller. The helix angle calculated to model the twist distribution in this model was 7.97°, showing that the methodology was relatively accurate. Moreover, by submitting the thrust, diameter and RPM requirements into JavaPro (36), an online propeller model generator, the recommended pitch at the 0.75r station was 13°, which closely correlates to the 13.97° used for the 0.1 diameter propeller.

L. Design of Best Case Model

Using the data available from all of the testing, it was clear that efficiency benefits were possible from reducing solidity, using the minimum number of propeller blades, incorporating a 9% thickness airfoil and mapping the geometric twist distribution using the modified method. Although the 5cm diameter propellers were the most efficient, from thrust output charts it was estimated that a 7cm diameter propeller would provide adequate thrust

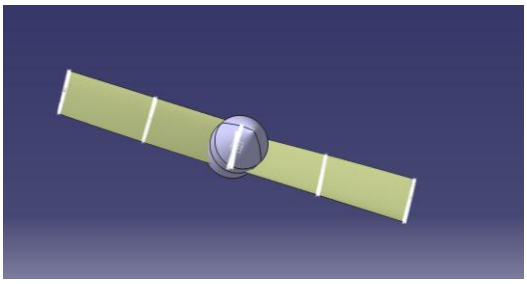

Figure 33. Original AR=8 propeller.

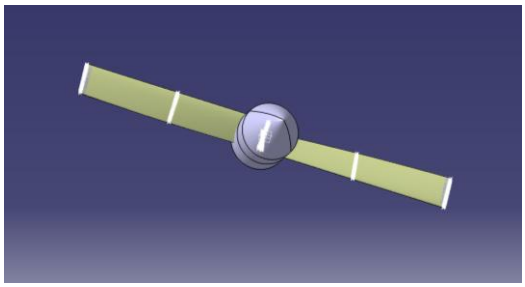

Figure 34. Optimised AR=12.3 propeller.

using the current blade aspect ratio of eight. However in order to reduce solidity further, it was decided to use an 8cm diameter propeller and reduce the blade chord length. The D=8cm propeller with AR=8 gave a thrust output of 0.384. Assuming an approximate proportionality between chord length and thrust produced, in order to produce 0.24N, the chord length must be reduced to 65% of the original length. This meant reducing the chord length from 10mm to 6.5mm, which yielded a new, higher aspect ratio of AR=12.3. The original and modified geometries can be compared in figures 33 and 34. The geometry was created with a NACA2309 airfoil using the modified twist distribution method, meshed, and tested in FLUENT over the usual range of advance ratios. The propeller efficiency, over a range of advance ratios, was compared against the NACA0007, NACA7207, and NACA2307, as shown below in figure 35. The optimised design had a maximum efficiency of 60.6% at $V_a = 13m/s$ and efficiency of 58.7% at the design advance velocity of $V_a = 11m/s$.

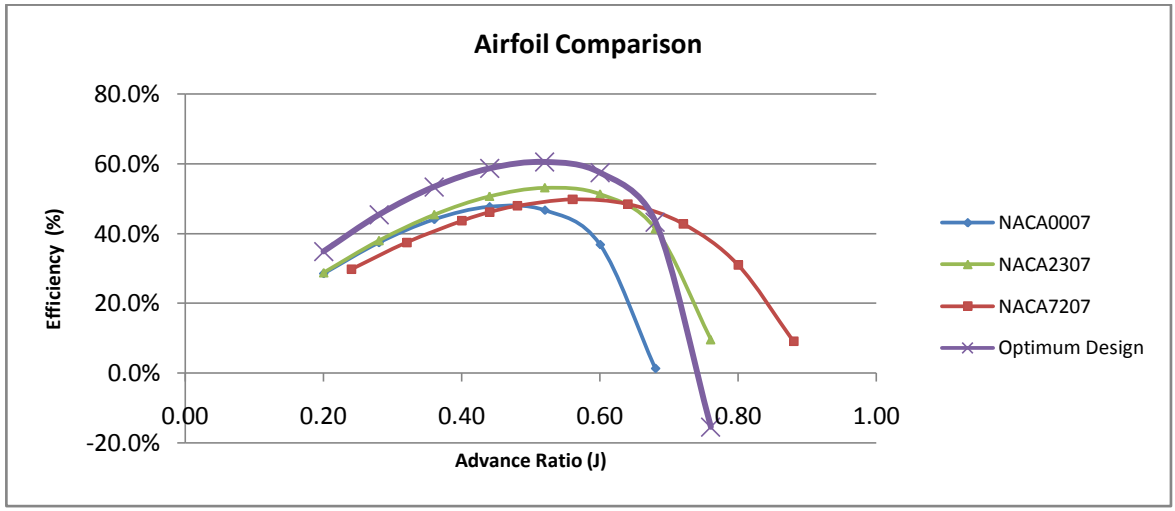

Figure 35. Comparison of optimized design to previous designs.

VII. Recommendations

A. Wind Tunnel Testing

The first and foremost recommendation from this report is that wind-tunnel validation of the results is undertaken. An excellent overview of and method for the wind-tunnel testing of small propellers can be found in Merchant's *Propeller Performance Measurement for Low Reynolds Number Unmanned Aerial Vehicle Applications* (15), a summary of which can be found in appendix K.

B. Combining non-linear twist and taper

This study has investigated the effect of some fundamental variables involved in the design of propellers; however the coupling of these variables pertaining to low-Re propeller efficiency is largely unknown. It is obvious that perhaps the most critical design parameter is the twist distribution, with thickness and general airfoil selection also having a significant impact on the propeller efficiency. At low advance ratios, maintaining low solidity and low blade loading helps to avoid the turbulent wake of the preceding blades in the flow and also significantly improves efficiency. However it is recommended that investigation into non-linear twist distributions are undertaken, comparing methodologies which aim to maintain each radial airfoil station at its most efficient condition, to methodologies which aim to generate the most uniform inflow through the propeller face. A common propeller blade parameter that has not been investigated in this study is blade taper. Taper reduces the solidity of the blades, particularly at the tips, which consequently reduces the inflow to the outer radial sections. This is desirable for efficiency as it creates a more uniform inflow. Since the twist directly influences the local lift and drag coefficients of the blade sections, an optimum combination for twist and taper may exist to provide the most uniform inflow along the blade span and higher propeller *T/Q*.

C. Radial Thickness Distribution

Many highly efficient propeller designs use a radial thickness distribution, for both wings and propeller blades, with thick airfoil sections near the hub and thin airfoil sections at the propeller tip. At the blade tips, where the angle of attack is often close to zero, the early separation characteristics of thin airfoils is no longer a problem in normal flight. A short 2D CFD study was completed to assess possible efficiency gains, by reducing airfoil thickness at tip from a NACA2308 to a NACA2303 airfoil (from 8% to 3% thickness). At an angle of attack of $\alpha = 0°$, the NACA2303 produced 9.61% less viscous drag and yielded a 8.90% greater *L/D* than a NACA2308 at the simulated tip speed of the 0.1m diameter propeller. Hence the use of thin airfoil tips, through a radial thickness distribution, can lead to greater efficiency. Likewise, if a radial geometric pitch distribution is used to create a uniform inflow, the blade angle of attack near the hub will be higher than near the tip, so thicker airfoils will be required to delay the onset of separation.

D. Sensitivity to Tip Design and Chord Distribution

Further geometric investigation is warranted in finding the sensitivity of efficiency to square vs rounded blade tips, spinner design and non-linear chord distributions, such as those found on the Black Widow propeller. A geometry was created to approximate the shape of the vaunted Black Widow propeller design, as shown in figure 36, incorporating a 15% to 5% thickness distribution from root to tip and four spline points instead of three. The intention was to run a 3D simulation on the model to assess its efficiency, unfortunately the geometry would not read correctly in FLUENT and no simulations could be run.

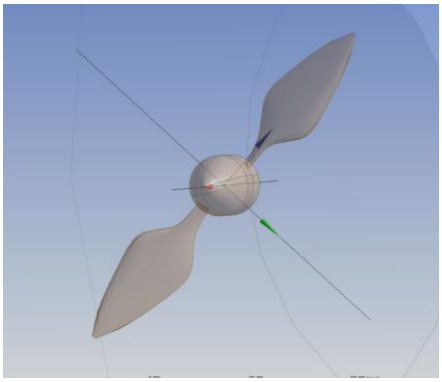

Figure 36. Attempted copy of Black Widow propeller.

E. Low-Re Airfoils

Some airfoils, such as the Eppler E174 and Selig S2060 airfoils, are designed specifically for low-Re flows, and their effectiveness in MAV flight regimes are worth investigating, both as MAV wings and propeller blades.

F. Alternate Propulsion Configurations

Three different propeller configurations warrant further investigation. They are the prop fan, the ducted propeller and the balanced single-blade propeller. Prop fan configurations, reminiscent of some very high solidity propeller configurations found on some Soviet aircraft, are geometrically complex, but offer significantly greater efficiency than turbo-fans between Mach 0.6-0.8 (3 p. 313). Between Mach 0.6-0.7, prop-fans are shown to be more efficient than turbo-props, although the trend beneath this speed is unknown. It is likely that their complex geometry will prove too difficult for application at MAV scale. The ducted propeller design vaunts uniform loading across the blade span and elimination of propeller rotational losses, however it adds weight and wetted area drag (3 p. 313). Finally, the 3D CFD testing revealed that the largest efficiencies were possible using a single-bladed propeller; however the 3D model did not include a counterweight which would have negative aerodynamic effects. If an aerodynamically acceptable method for balancing the single propeller blade is designed, it may offer MAV propulsion significantly greater propulsive efficiencies.

G. Dual Propellers

In this study the concept of propulsion delivered by a single propeller was investigated. There are however, many advantages to using twin propellers that warrant further investigation. Firstly, twin propellers, fitted at the leading edge of each wing, are likely to cover the entire MAV wing surface with energised flow from their wakes, which may promote better attachment in the low-Re flight regimes. Secondly, counter-rotating propellers will negate propeller torque effects, which is significant as control and stability for MAVs is exceptionally difficult. Thirdly, propellers positioned at the MAV wingtips offer unique aerodynamic advantages known as the Zimmelman effect. If the propeller helical slipstream is set-to counter the wingtip vortices, the slipstream can negate somewhat the strength of these vortices and reduce the induced drag, effectively increasing the wing aspect ratio (1).

H. Non-axial Flows

Finally, it is recommended that the effect of off-axis flows on the propulsive efficiency be investigated for these low-Re propellers, as wind buffeting and yaw will be common flight conditions for a MAV.

VIII. Conclusions

The following conclusions were drawn from this CFD investigation on MAV propeller aerodynamics:

a. For $Re < 30{,}000$, airfoil and propeller performance deteriorates rapidly as viscous forces gain dominance and laminar flow separation becomes more prevalent.
b. Literature suggests massive flow separation and laminar separation bubbles are largely responsible for poor aerodynamic performance of conventional airfoils at low-Re.
c. A CFD model using a moving cylindrical reference frame containing a propeller geometry, connecting to a fluid interface, is an accurate and effective method for determining propeller performance, as validated by Roskam's estimation methods.
d. A polyhedral mesh conversion was necessary for the 3D propeller analysis due to the massive numbers of grid elements involved.
e. The propellers designed performed better at higher advance ratios than the design point, or where the propeller stations were subject to a smaller angle of attack than intended.
f. For a certain angle of attack, there exists a *t/c* which will give the highest airfoil *L/D*. Higher angles of attack favour thicker airfoil sections. There also exists an angle of attack for each airfoil which gives a maximum *L/D*, this is usually between 5-7°.
g. At low-Re, cambered airfoils offer significant improvements in performance for both airfoils (*L/D*) and propellers (*T/Q*) than uncambered airfoils.
h. The optimal 2D airfoil design, a NACA7207, was not found to give the best efficiency when used on a 3D propeller, for which a NACA2307 airfoil provided higher efficiency. Furthermore, a 9% thick airfoil offered greater performance than a 7% *t/c* airfoil in the 3D model. The 2D results assisted in identifying trends but optimum cases did not correspond directly when used in the 3D model. A significant amount of work can still be done to identify optimal propeller airfoils.
i. Low-Re propeller efficiency is highly sensitive to solidity at low advance ratios. Because small propellers generally operate at high RPMs, high solidity ratios lead to interference by turbulence wakes and degrade performance significantly. The optimal number of propeller blades investigated was found to be one, in terms of efficiency, however this comes with a range of mechanical issues including use of a counter-balance which has not been examined in this study. For this reason, a 2-bladed propeller is recommended for use on the MAV.
j. High blade loadings cause a reduction in propeller efficiency; however blade loading should not be reduced at the expense of adding propeller blades, the negative effects of which greatly outweigh the slight efficiency increase attained by reducing P_{bl}. For this reason, the most efficient propeller geometry tested was a 2-bladed design with a 5cm diameter; however inadequate thrust is generated at 20,000RPM at the required flight speed until diameters of 7-8cm are used, depending on the blade aspect ratio.
k. A linear geometric pitch-distribution based on maintaining a 6° angle of attack at the 0.75r station, and a 0° angle of attack at the blade tip, offered significant efficiency improvements. This was particularly evident at higher advance ratios, over a linear distribution which maintained a 6° angle of attack at both the 0.45r and 0.75r stations.
l. An optimal propeller design was based upon generating the required thrust to propel the MAV by using an 8cm diameter operating at 20,000RPM. The blade solidity was reduced by increasing the blade aspect ratio to 12.3 from the *AR*=8 used in all other tests in this study. The propeller used the improved geometric twist distribution and a NACA2309 airfoil and yielded an overall maximum efficiency of 60.6% at 13m/s, or an advance ratio of 0.52. The efficiency at the forward speed design point of 11m/s

was 58.7%. This is comparable to the 63% efficiency of the direct drive propeller used by the Black Widow.

m. Further optimisation of the propeller blade geometry will involve a radial thickness distribution, a non-linear radial geometric pitch distribution, and perhaps a non-linear radial chord distribution to maximise Reynolds numbers over lift generating areas, reduce blade-tip vortices and create uniform inflow.

n. Further investigation is also warranted into the performance of a large range of existing low-Re airfoils, such as the Eppler E174; testing of off-design inlet flows experienced during aircraft yaw and wind gusts, use of ducting over the propeller, a balanced single-blade prop, and performance of prop-fan designs; and

o. Wind tunnel testing is ultimately required to verify the trends identified in this CFD investigation.

Micro-air vehicles are aircraft which operate in flow regimes with Reynolds numbers far smaller than full-scale aircraft. The radial stations of MAV propellers typically operate within $5{,}000 \leq Re \leq 100{,}000$, for which the aerodynamics are characterised by laminar flow which separates before turbulent transition and reattachment. The propulsive efficiency of propellers used provide thrust to these MAVs can vary considerably depending on the design of the blades, yet little information is available to assist the engineer in optimising a propeller for a given platform. The aim of this study was to test a range of propeller design variables such as the effect of airfoil thickness, camber position, camber percentage and Reynolds number regime on *L/D*, and 3D propeller designs were tested by varying airfoil type, thickness, diameter, number of blades and radial twist distribution. The information gathered from these comparisons was to allow the creation of an optimum propeller design which satisfied the requirements to provide 0.24N of thrust with a propeller efficiency greater than 50% at 20,000RPM for a forward speed of 11m/s. It is unlikely that the 10° climb thrust requirement can be met without significantly increasing propeller RPM, which will have an adverse effect on efficiency. Regardless, the final design is suitable to propel a MAV platform with a wingspan of 150mm and a take-off weight of 150 grams. Further efficiency gains may be made after implementing some of the above recommendations. This study involved over 200 2D tests and over 230 3D tests, totalling approximately 1900 hours of computation time for meshing, converting mesh domains to polyhedra in 3D models, and calculation time. This excludes the time spent creating, and importing geometries, and applying CFD settings.

Acknowledgements

A great number of people have invested their time and their lives in bringing my undergraduate study to a close, to which I am eternally indebted. First and foremost I would like to acknowledge my supervisor Dr Rikard Heslehurst, whose mentoring and example made my thesis a rewarding and enjoyable experience. Furthermore, his courses on aircraft design were among the most interesting and practical that I completed during my time at UNSW@ADFA, and without which I couldn't complete this project. Similarly, Dr John Young provided the CFD tools for me to undertake this study on MAV propellers by delivering a course on Computational Fluid Dynamics in the first semester of 2010, and then spent many hours in the computer labs with me, providing advice and assisting with FLUENT and the design of my 3D model. It is certain that this project would not be possible without his expertise and I am very grateful for his willingness to invest his time in students. In terms of tools, the ADFA School of Engineering and Information Technology made the sheer number of CFD tests possible through their vast computer resources and newly upgraded platforms. I would like to thank Dr Michael Harrap for providing some very insightful and helpful feedback in both my viva and seminar which has been addressed in this report. A mention should also be made to Dr Andrew Neely who assisted the entire course through his Thursday afternoon thesis prep lessons, and did for me a great favour by allowing me to postpone my thesis seminar to a later date when I was preoccupied with other commitments. I would also like to acknowledge Dr Jan Roskam, Dr Daniel P. Raymer and Professor John D. Anderson, legends in their fields, and primary references not only for this paper, but for my entire undergraduate degree. To my friends and fellow aeronautical engineering students, thank you for your support and tireless humour. Particularly I would like to acknowledge David Ghali for his Excel expertise, and ability to know exactly when to order me late meals from the Officers Mess; Aidan Watters for his morale port, and ability to look at any problem in Excel or CATIA and know exactly how to fix it; and James Walduck, my closest friend, and entertaining lab partner for literally the hundreds of hours spent in front of iterating FLUENT residuals. In Dayne Schmidt I could not ask for a better roommate, and whose relaxed attitude and excellent taste in music helped make long hours of study all the more bearable. Finally, Hayley Achurch and Tracy Douglas, such important ladies in my life, who listened to my frustrations, opened their houses, and whisked me off base at opportune moments to share life and take a break from study. To a great extent, I am only finishing my BE(Aero) and graduating from ADFA because of Tracy and the long-ago motivating words of a wise man named Darren Fisher.

Works Cited

1. **Mueller, Thomas J, et al.** *Introduction to the design of fixed-wing micro air vehicles.* Blacksburg, Virginia : American Institute of Aeronautics and Astronautics, 2006.
2. Good things come in small packages: the new UAV family. *Jane's Online.* [Online] 08 April 2010. [Cited: 20 April 2010.] http://search.janes.com/Search/documentView.do?docId=/content1/janesdata/mags/idr/history/idr2010/idr12983.htm@current&pageSelected=allJanes&keyword=wasp micro&backPath=http://search.janes.com/Search&Prod_Name=IDR&.
3. **Roskam, J and Chuan-Tau, E.L.** *Airplane aerodynamics and performance.* Lawrence, Kansas : DARcorporation, 2008.
4. **Barnhart, Francis, et al.** *Micro-aerial vehicle design with low reynolds number airfoils.* 2004.
5. **Hacker Brushless Motors.** *Brushless-Motors A10-Motors.* [PDF document] Niederhummel : Hacker Motor GmbH, 2007.
6. Jane's Unmanned Aerial Vehicles and Targets. *Janes Online.* [Online] 23 Mar 2009. [Cited: 12 March 2010.]
7. NightHawk - Miniature UAV. *Ddefence Update Online Defence Magazine.* [Online] 2009. [Cited: 04 April 2010.] http://defense-update.com/products/n/nighthawk.htm.
8. Nighthawk Micro Air Vehicle (MAV). *ARA Robotics.* [Online] 2010. [Cited: 04 April 2010.] http://www.ara.com/robotics/Nighthawk.html.
9. **Grasmeyer, J.M and Keennon, M.T.** *Development of the Black Widow micro air vehicle.* Simi Valley : AeroVironment, Inc, 2001. AIAA-2001-0127.
10. *Propelling the 1903.* **Hiemcke, Christophe.** 2003, Fluent NEWS, pp. 6-7.
11. **Delp, Frank.** *Aircraft propellers and controls.* Frankfurt : Jeppesen & Co, 1979. 92-24615.
12. **Hepperle, Martin.** How a propeller works. *Propulsion by propellers.* [Online] 6 November 1996. [Cited: 20 March 2010.] http://www.mh-aerotools.de/airfoils/propuls4.htm.
13. Blade element and momentum theory. *Helis.com.* [Online] [Cited: 15 April 2010.] http://www.helis.com/howflies/bet.php.
14. *Small rotor design optimisation using blade element momentum theory and hover tests.* **Bohorquez, Felipe, Pines, Darryll and Samuel, Paul D.** 1, Maryland : Journal of Aircraft, 2010, Vol. 47.
15. **Merchant, Monal P.** *Propeller performance measurement for low reynolds number unmanned aerial vehicle applications.* Wichita : Wichita State University, 2004.
16. *Low reynolds number airfoil survey.* **Carmichael, B.H.** Nov 1981, s.l. : NASA CR, Vol. 1.
17. **Eppler, R and Hepperle, M.** *A procedure for propeller design by inverse methods.* Stuttgart : Universitat Stuttgart, 2003.
18. **Hepperle, Martin.** Design of a propeller. *Aerodynamics for model aircraft.* [Online] 2006. [Cited: 2 June 2010.] http://www.mh-aerotools.de/airfoils/jp_propeller_design.htm.
19. **Crigler, J.L.** *Application of Theodorsen's theory to propeller design.* Langley Field : National Advisory Committee for Aeronautics, 1948.
20. Propellers for small UAVs. [Online] Barnard Microsystems Limited, 2010. [Cited: 26 August 2010.] http://www.barnardmicrosystems.com/L4E_propellers.htm.
21. **Weick, Fred.** *Propeller Design: Practical application of the blade element theory - I.* Washington : National Advisory Committee for Aeronautics, 1926.
22. **Price, David.** *NACA four-digit airfoil profile.* [Microsoft Excel document] 2010.
23. **Raymer, Daniel P.** *Aircraft design: a conceptual approach.* Virginia : American Institute of Aeronautics and Astronautics, Inc., 2006. 1-56347-829-3.
24. *CFD simulation of propeller and rudder performance when using additional thrust fins.* **Sheng, H, et al.** Vol.6, No.4, December 2007, Journal of Marine Science and Applications, pp. 27-31.
25. **ANSYS.** *DesignModeler.* [PDF document] s.l. : ANSYS, Inc. Proprietary, 2009.
26. *ANSYS: Introduction to FLUENT.* [PDF document] s.l. : ANSYS, Inc. Proprietary, 2009.
27. *Analysis of screw propeller 4119 using the Fluent system.* **Kulczyk, J, Skraburski, L and Zawislak, M.** 4, Wroclaw : Archives of Civil and Mechanical Engineering, 2007, Vol. VII.
28. **Ghali, David.** *MAV Wing Template: Thesis 2010.* [Microsoft Excel document] Canberra : s.n., 2010.
29. Running ANSYS CFX. *ANSYS CFX, Release 11.0.* [Online] ANSYS. [Cited: 12 September 2010.] http://www.kxcad.net/ansys/ANSYS_CFX/help/help/Intro/i1337501.html.
30. **Anderson, John. D.** *Introduction to Flight.* New York : McGraw-Hill, 2005.
31. *Mesh optimization for ground vehicle aerodynamics.* **Ahmad, N.E, Essam, A and Gaylard, A.** Vol. 2(1) 2010, CFD Letters, pp. 54-65.
32. **Peric, M and Ferguson, S.** The advantage of polyhedral meshes. *CD-adapco.* [Online] 2010. [Cited: 15 August 2010.] http://www.cd-adapco.com/press_room/dynamics/24/testVspoly.html.

33. **National Aeronautics and Space Administration.** Mach number: role in compressible flows. *NASA Glenn Research Center*. [Online] 29 July 2008. [Cited: 21 July 2010.] http://www.grc.nasa.gov/WWW/BGH/machrole.html.
34. **Aki, M, Waszak, M and Shkarayev, S.** Development of micro air vehicles with in-flight adaptive wing. [book auth.] T.J Mueller, et al. *Introduction to the design of fixed-wing micro air vehicles.* Tucson, Arizona : American Institute of Aeronautics and Astronautics, Inc., 2006, pp. 241-275.
35. **Lednicer, David.** An incomplete guide to airfoil usage. [Online] Raisbeck Engineering, September 2010. [Cited: 21 May 2010.] http://www.ae.illinois.edu/m-selig/ads/aircraft.html#helicopters.
36. **Hepperle, Martin.** JavaProp - Design and Analysis of Propellers. *Aerodynamics for Model Aircraft*. [Online] 2006. [Cited: 24 March 2010.] http://www.mh-aerotools.de/airfoils/javaprop.htm.
37. Typical lift coefficient on an RC airplane? *RC Universe*. [Online] 22 April 2009. [Cited: 20 April 2010.] http://www.rcuniverse.com/forum/m_8704122/printable.htm.
38. **McIver, John.** *Cessna Skyhawk II/100 Performance Assessment.* [Online Document] s.l. : Temporal Images, 2003.
39. Aerospace, Civil & Mechanical Engineering Laboratories. *UNSW@ADFA*. [Online] 09 August 2005. [Cited: 20 April 2010.] http://ftp.adfa.edu.au/acme/facilities/laboratories.html.
40. **Pope, Alan and Harper, John J.** *Low-speed wind tunnel testing.* Sydney : John Wiley & Sons, Inc., 1966.
41. Strobotac. *Electrical Engineering Training Series*. [Online] Integrated Publishing. [Cited: 20 April 2010.] http://www.tpub.com/neets/book16/67c.htm.
42. *Application of CFD in analysis of conventional propeller and azimuth thruster*. **Amoraritei, Mihaela.** Timisoara : Politehnica University of Timisoara, 2005.
43. **Sharma, P and Dubey, D.** *Drag analysis of mini air vehicles.* Bombay : Indian Institute of Technology, 2004.
44. The lifting fuselage body. *Aeronautics*. [Online] Meridian International Research, 22 September 2005. [Cited: 28 April 2010.] http://www.meridian-int-res.com/Aeronautics/Burnelli.htm.
45. **Maynard, J.D and Steinberg, S.** *Report 1126: the effect of blade-section thickness ratios on the aerodynamic characteristics of related full-scale propellers at mach numbrs up to 0.65.* Langley Field : National Advisory Committee for Aeronautics, 1949.
46. Brushless Motor with Propeller and Speed Controller. *www.robokits.co.in*. [Online] 2008. [Cited: 15 October 2010.] http://robokits.co.in/shop/index.